



**HAL**  
open science

# Hydroperoxide Measurements During Low-Temperature Gas-Phase Oxidation of n-Heptane and n-Decane

Anne Rodriguez, Olivier Herbinet, Xiangzan Meng, Christa Fittschen, Zhandong Wang, Lili Xing, Lidong Zhang, Frédérique Battin-Leclerc

► **To cite this version:**

Anne Rodriguez, Olivier Herbinet, Xiangzan Meng, Christa Fittschen, Zhandong Wang, et al.. Hydroperoxide Measurements During Low-Temperature Gas-Phase Oxidation of n-Heptane and n-Decane. *Journal of Physical Chemistry A*, 2017, 121 (9), pp.1861-1876. 10.1021/acs.jpca.6b10378 . hal-01676244

**HAL Id: hal-01676244**

**<https://hal.science/hal-01676244v1>**

Submitted on 5 Jan 2018

**HAL** is a multi-disciplinary open access archive for the deposit and dissemination of scientific research documents, whether they are published or not. The documents may come from teaching and research institutions in France or abroad, or from public or private research centers.

L'archive ouverte pluridisciplinaire **HAL**, est destinée au dépôt et à la diffusion de documents scientifiques de niveau recherche, publiés ou non, émanant des établissements d'enseignement et de recherche français ou étrangers, des laboratoires publics ou privés.

# Hydroperoxide Measurements During Low-Temperature Gas-Phase Oxidation of *n*-Heptane and *n*-Decane

Anne Rodriguez<sup>1</sup>, Olivier Herbinet<sup>1</sup>, Xiangzan Meng<sup>1,2</sup>, Christa Fittschen<sup>3</sup>, Zhandong Wang<sup>4,\*</sup>, Lili Xing<sup>4</sup>, Lidong Zhang<sup>4</sup>, and Frédérique Battin-Leclerc<sup>1,\*\*</sup>

<sup>1</sup>Laboratoire de Réactions et Génie des Procédés, CNRS–Université de Lorraine, ENSIC, 1 rue Grandville, 54001 Nancy, France

<sup>2</sup>State Key Laboratory of Engines, Tianjin University, Tianjin 300072, China

<sup>3</sup>Université Lille, CNRS, UMR 8522 - PC2A - Physicochimie des Processus de Combustion et de l'Atmosphère, F-59000 Lille, France

<sup>4</sup>National Synchrotron Radiation Laboratory, University of Science and Technology of China, Hefei, Anhui 230029, P. R. China

Published in *J. Phys. Chem. A*, 2017, 121 (9), 1861–1876  
[10.1021/acs.jpca.6b10378](https://doi.org/10.1021/acs.jpca.6b10378)

## Abstract

A wide range of hydroperoxides (C<sub>1</sub>–C<sub>3</sub> alkyl hydroperoxides, C<sub>3</sub>–C<sub>7</sub> alkenyl hydroperoxides, C<sub>7</sub> ketohydroperoxides, and hydrogen peroxide (H<sub>2</sub>O<sub>2</sub>)), as well as ketene and diones, have been quantified during the gas-phase oxidation of *n*-heptane. Some of these species, as well as C<sub>10</sub> alkenyl hydroperoxides and ketohydroperoxides, were also measured during the oxidation of *n*-decane. These experiments were performed using an atmospheric-pressure jet-stirred reactor at temperatures from 500 to 1100 K and one of three analytical methods, time-of-flight mass spectrometry combined with tunable synchrotron photoionization with a molecular beam sampling; time-of-flight mass spectrometry combined with laser photoionization with a capillary tube sampling, continuous wave cavity ring-down spectroscopy with sonic probe sampling. The experimental temperature at which the maximum mole fraction is observed increases significantly for alkyl hydroperoxides, alkenyl hydroperoxides, and then more so again for hydrogen peroxide, compared to ketohydroperoxides. The influence of the equivalence ratio from 0.25 to 4 on the formation of these peroxides has been studied during *n*-heptane oxidation. The up-to-date detailed kinetic oxidation models for *n*-heptane and for *n*-decane found in the literature have been used to discuss the possible pathways by which these peroxides, ketene, and diones are formed. In general, the model predicts well the reactivity of the two fuels, as well as the formation of major intermediates.

\* Author Present Address: King Abdullah University of Science and Technology (KAUST), Clean Combustion Research Center (CCRC), Thuwal 23955–6900, Saudi Arabia.

\*\* Corresponding author information: E-mail: frederique.battin-leclerc@univ-lorraine.fr. Phone: +33 3 83 17 51 25

## Introduction

Hydroperoxides are major chain-branching agents that explain the occurrence of hydrocarbon autoignition. Since 2010, the detection of these highly reactive intermediates has been increasingly reported during hydrocarbon gas-phase oxidation.<sup>1</sup> This is the case of alkyhydroperoxides,<sup>2,11</sup> ketohydroperoxides,<sup>2-6,11</sup> and hydrogen peroxide.<sup>5,7-11</sup> Most of the experimental studies reported have been performed using a jet-stirred reactor (JSR), a type of reactor extremely suitable for reaction product quantification and kinetic modeling.<sup>12</sup>

*n*-Heptane (C<sub>7</sub>H<sub>16</sub>) is a primary reference fuel used for octane rating in spark ignited engines.<sup>13</sup> *n*-Decane (C<sub>10</sub>H<sub>22</sub>) is often considered as a surrogate for long linear alkanes present in diesel fuel.<sup>14</sup> The gas-phase oxidation of these two *n*-alkanes has already been thoroughly investigated experimentally, and many models have been proposed.<sup>15</sup> However, only one paper<sup>3</sup> concerns hydroperoxide formation during *n*-heptane oxidation: ketohydroperoxides formed under stoichiometric conditions were detected using a tunable synchrotron vacuum ultraviolet photoionization mass spectrometer (SVUV-PIMS). To our knowledge, no peroxide measurement has yet been published for *n*-decane gas-phase oxidation.

As a first objective, this paper investigated the low-temperature oxidation of *n*-heptane in JSR at atmospheric pressure covering a wide range of equivalence ratios ( $\varphi$ : 0.25, 1, 2, and 4). This was especially performed using two analytical methods that have not very often been coupled to JSRs: time-of-flight mass spectrometry combined with laser single-photon photoionization (SPI) and continuous wave cavity ring-down spectroscopy (cw-CRDS). These two methods allowed hydroperoxides to be detected without the use of a synchrotron, enabling us to use them in Nancy. This work extended our previous study that showed peroxide measurements during JSR *n*-heptane oxidation.<sup>3</sup> The second objective of the current work was to extend the *n*-heptane measurements to the case of a larger alkane, *n*-decane. This was also performed at atmospheric pressure, but only for a stoichiometric mixture.

The full analyses by gas chromatography (GC) of the reaction products obtained upon JSR *n*-heptane oxidation for the same conditions as in the present work can be found in Zhang et al.<sup>16</sup> and Herbinet et al.<sup>3</sup> Figure S1 shows the fuel consumption observed by GC during these previous studies.<sup>3,16</sup> Concerning *n*-decane, a full GC analysis was recently published by Herbinet et al.<sup>17</sup> for an equivalence ratio of 0.41 (inlet *n*-decane mole fraction = 0.025). In the present study, we performed some GC measurements under stoichiometric conditions for the same initial fuel mole fraction, to assist the SPI mass spectrometry study of *n*-decane. The GC method and related uncertainties are described in Supporting Information. Figure S1 also plots the details of *n*-decane consumption observed by GC during JSR *n*-decane oxidation under stoichiometric conditions.

## Experimental Details and Calculations

The experimental work was performed using a spherical fused silica JSR (volume of 85 cm<sup>3</sup>) already described in the literature.<sup>12</sup> Diluted reagents entered the reactor through an injection cross located at its center. The gas jets provoked high turbulence leading to homogeneity in composition and temperature of the gas phase. The isothermal JSR was preceded by a quartz annular preheated zone in which the gaseous temperature was increased up to that of the reactor. The gas mixture residence

time inside the annular preheater was very short compared to its residence time inside the reactor (only a few percentiles). Both the reactor and the preheating zone were heated by Thermocoax resistances rolled up around the reactor. The reaction temperature was measured by a thermocouple located inside the intra-annular space of the preheating zone; its tip being placed in a glass finger at the level of the injection jets.

In France, oxygen and helium were provided by Messer, and their purities were reported as 99.995 and 99.999%, respectively. Both fuels were provided by Sigma-Aldrich (purity of  $\geq 99\%$ ). In China, gases were provided by Nanjing Special Gas Factory Co., Ltd. Purities of argon and oxygen were 99.99% and 99.999%, respectively; *n*-heptane and *n*-decane were purchased from Aladdin Reagent Co., Ltd. with a purity of 99%. Gas flow rates were controlled by mass flow controllers, and Coriolis flow controllers were used for liquid fuels. The uncertainty in the flow measurements is  $\sim 0.5\%$  for each controller. In all experiments, the residence time was equal to  $2 \pm 0.04$  s.

The inlet *n*-heptane mole fraction was 0.005 in all experiments, while the inlet *n*-decane mole fraction was 0.0025 in the experiment combined with SPI mass spectrometry and GC. These inlet mole fractions were chosen to allow close reactivity to be observed for both fuels under stoichiometric conditions (see Figure S1). For the *n*-decane SVUV-PIMS experiment, an inlet fuel mole fraction of 0.004 was chosen to obtain a more accurate determination of the ionization energy of some detected products. Figure S1 also plots the *n*-decane consumption observed by SVUV-PIMS during JSR *n*-decane oxidation under these less-diluted conditions.

The JSR described below has been associated with three types of analytical setup:

- A reflectron time-of-flight mass spectrometer combined with tunable synchrotron vacuum ultraviolet photoionization (SVUV-PIMS) using molecular-beam sampling in Hefei.
- A laser single-photon-ionization time-of-flight mass spectrometer (SPI-MS) through capillary-tube sampling in Nancy.
- A continuous wave cavity ring-down spectroscopy (cw-CRDS) optical cell via a sonic probe in Nancy.

In most cases, the carbon atom balance of the reactants and products is within 90%. We observe large deviations in *n*-decane oxidation at temperatures close to the maximum of low-temperature reactivity. This is probably due to the formation of undetected large oxygenated products.

### ***SVUV-PIMS Analyses***

The SVUV-PIMS analyses and the coupling with JSR through a molecular beam have been described previously.<sup>2,3,18-20</sup> Briefly JSR was coupled to the low-pressure photoionization chamber through a lateral fused silica conelike nozzle, which was inserted into the spherical part of the reactor. The tip of the cone was pierced by a 50  $\mu\text{m}$  orifice. A nickel skimmer with a 1.25 mm diameter aperture was located 15 mm downstream from the sampling nozzle. The ion signal was detected with the reflectron time-of-flight mass spectrometer (RTOF-MS), which was installed vertically above the photoionization chamber. For a detailed description of this experimental apparatus and the related calibration see ref 2. In the case of *n*-heptane, most of the SVUV-PIMS data have already been published in ref 3. However, some unpublished data obtained with this system are shown here,

serving for product identification and comparison purposes. In addition, H<sub>2</sub>O<sub>2</sub> data were reevaluated using the photoionization cross sections recently proposed by Dodson et al.<sup>21</sup> Here the same apparatus was used to analyze the *n*-decane oxidation with inlet mole fraction of 0.004 and equivalence ratio of 1.0. The purpose of this experiment is to help identify several intermediates and assist the SPI-MS analysis.

### SPI-MS Analyses

These experiments were performed using an RTOF-MS equipped with a dual ion source for electron-impact and single-photon ionizations (PhotoTOF, Photonion GmbH, Germany, a custom-device developed for LRGP-Nancy). This mass spectrometer was previously used to analyze the outlet gas from fast pyrolysis of biomass performed in a microfluidized bed reactor.<sup>22</sup> As is shown in Figure 1, products were sampled using a heated quartz capillary tube (200 μm diameter, 5 m length, flow of 3–4 mL/min), which was inserted directly within the JSR. The whole sampling line was heated to 363 K when using both fuels. This temperature was carefully chosen after testing several sampling line temperatures to preserve hydroperoxides and to maximize the signal obtained despite a high tendency of reagents with a weak O–O bond to decompose. At the outlet of the heated capillary line, compounds were directly injected into the ionization zone of the mass spectrometer. In the measurements described here, VUV photons with a wavelength of 118 nm (10.6 eV) were used for a single-photon absorption/ionization process. The mass spectrometer covers a mass range of *m/z* 10–2000 with mass resolution of 2000 and mass sensitivity of 100 ppb.

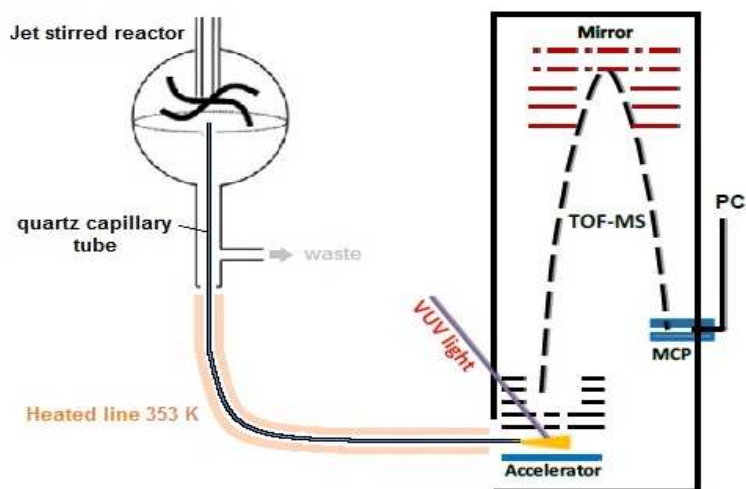


Figure 1. Schematic diagram of the instruments including the JSR and the laser photoionization mass spectrometer.

Since no molecular beam was involved in the sampling procedure, the signal calibration was simpler than that when using SVUV-PIMS.<sup>2</sup> The mole fraction of a species, *i*, was directly obtained from that of a reference species, *ref*, at a given temperature and laser energy by the equation:

$$\frac{S_i(T)}{S_{ref}(T)} = \frac{X_i(T)}{X_{ref}(T)} \cdot \frac{\sigma_i(T)}{\sigma_{ref}(T)} \quad (1)$$

The chosen reference was propene at  $m/z$  42 using the value measured by gas chromatography at 650 K.<sup>16</sup> More details about the ionization cross sections used are given in Supporting Information. For compounds with unknown cross sections, estimation was made based on the group additivity method proposed by Bobeldijk et al.<sup>23</sup> Groups are defined as bonded atom pairs (see Supporting Information) in the considered molecules, except that C–H, O–H, and O–O pairs are not counted. The value of each group is estimated from published data of known species<sup>24–27</sup> at a given photon energy and is given in Supporting Information. From there, the cross section is obtained as the sum of each group constituting the related molecule. As an example, we have for the C7 ketohydroperoxide shown in Scheme S1 of Supporting Information:

$$\sigma_{keto} = 6. \sigma_{C-C} + 1. \sigma_{C-O} + 1. \sigma_{O-O} + 1. \sigma_{C=O}$$

As shown in Supporting Information, the uncertainty on cross sections estimated by this method is assumed to be below 50%. However, small molecules with ionization energy above 10.6 eV cannot be detected by the SPI-MS used in this work. The quantification of the fuel is also difficult because of the saturation of the signal.

### ***cw-CRDS Analyses***

The same experimental setup has been used in previous studies of the oxidation of methane,<sup>28</sup> *n*-butane,<sup>7,8</sup> *n*-pentane,<sup>11</sup> and dimethyl ether.<sup>29</sup> The atmospheric-pressure JSR is coupled to a tubular-glass cw-CRDS cell (length: 86 cm, diameter: 0.8 cm, maintained at a pressure of 1.33 kPa through pumping at both ends) using a tubular quartz probe with a tip orifice of  $\sim 150$   $\mu\text{m}$  diameter. CRDS analyses<sup>30,31</sup> were performed in the near-infrared with wavenumbers in the 6620–6644  $\text{cm}^{-1}$  range (more details are given in Supporting Information). In addition to  $\text{H}_2\text{O}_2$ , several other species such as  $\text{H}_2\text{O}$ ,  $\text{CH}_2\text{O}$ , and  $\text{C}_2\text{H}_4$  could be quantified using this technique, as isolated absorption lines could be identified. The absorption lines used are given in Table 1.  $\text{H}_2\text{O}_2$  absorption cross sections for several lines have been obtained in separate experiments where the  $\text{H}_2\text{O}_2$  concentration has been derived from OH decays measured by time-resolved laser-induced fluorescence following  $\text{H}_2\text{O}_2$  photolysis.<sup>32</sup>

Table 1. Absorption Lines and Cross Sections Used for the Quantification of Formaldehyde, Ethylene, Water, and Hydrogen Peroxide

	wavenumber $\nu$ ( $\text{cm}^{-1}$ )	cross section $\sigma$ ( $\text{cm}^2$ )	reference
$\text{CH}_2\text{O}^a$	6639.33	$3.60 \times 10^{-22}$	Morajkar et al. <sup>30</sup>
	6641.67	$4.59 \times 10^{-22}$	
$\text{H}_2\text{O}$	6638.9	$4.46 \times 10^{-23}$	Macko et al. <sup>31</sup>
	6640.9	$1.60 \times 10^{-22}$	
$\text{H}_2\text{O}_2$	6639.26	$7.62 \times 10^{-23}$	Parker et al. <sup>32</sup>
	6640.06	$1.41 \times 10^{-22}$	
$\text{C}_2\text{H}_4$	6638.33	$4.05 \times 10^{-23}$	Bahrini et al. <sup>8</sup>
	6641.23	$2.95 \times 10^{-23}$	

<sup>a</sup> The mole fraction of a compound at a given temperature is calculated as the average of the mole fractions calculated using each line.

### ***Uncertainties Related to MS and CRDS Analyses***

The uncertainties related to photoionization mass-spectrometry measurements are mainly due to uncertainties in the photoionization cross sections (PICSs) used. For mole fractions evaluated from SVUV-PIMS signals, these uncertainties are usually estimated as  $\pm 10\%$  for major species,  $\pm 25\%$  for intermediates with known PICSs, and at least a factor of 2 for those with estimated PICSs,<sup>33</sup> as it is the case for hydroperoxides. The uncertainties for mole fractions evaluated from SPI-MS signals are estimated in a similar way.

To give a clearer idea of the uncertainty concerning SPI-MS data, the species yields were determined as a function of temperature upon JSR experiments for several habitual combustion products formed during *n*-heptane oxidation under stoichiometric conditions and are given in Figure 2, for example, propene ( $m/z = 42$ , the quantification was not possible between 875 and 900 K due to peak saturation), acetaldehyde ( $m/z = 44$ ), butenes ( $m/z = 56$ ),  $C_3H_6O$  isomers ( $m/z = 58$ ), and  $C_4H_8O$  isomers ( $m/z = 72$ , the quantification was not possible between 580 and 700 K due to peak saturation). The products shown in Figure 2 have an ionization energy below 10.6 eV allowing them to be detected using SPI-MS. Butenes,  $C_3H_6O$  isomers, and  $C_4H_8O$  isomers were quantified using the PICS of 1-butene, propanal, and butanal, respectively. These profiles are compared with the GC measurements of Zhang et al.<sup>16</sup> and with the SVUV-PIMS profiles of Herbinet et al.<sup>3</sup> (measurements were only made between 500 and 750 K). The mole fractions of propene and acetaldehyde measured by both mass spectrometry techniques agree very well with GC measurements. The comparison between GC and SPI-MS is also robust for butenes, as well as for  $C_3H_6O$  isomers and  $C_4H_8O$  isomers. Figure 2 also shows a comparison of SPI-MS data with our new GC measurements for propene and butenes during *n*-decane oxidation. A satisfactory agreement is observed. In the *n*-decane oxidation experiments, the accurate GC quantifications of acetaldehyde were not possible due to peak coelution with that of methanol (the peak separation was better in the case of *n*-heptane).  $C_3H_6O$  and  $C_4H_8O$  isomers are also not shown for *n*-decane, because, due to a much lower fuel concentration, the related isomers are more difficult to quantify by GC than those of *n*-heptane oxidation or in our previous work with *n*-pentane.<sup>11</sup> This is also caused by the coelution and/or signal intensity close to the limit of detection.

Uncertainties in mole fractions derived from CRDS measurements are mainly due to absorption cross section and measured ring down time uncertainties. The average uncertainty in mole fractions is estimated at 15% depending on the absorption line and the species concentration. In some cases, higher uncertainties can be observed due to line saturation. The detection limit depends on the intensity of the absorption line ( $\sim 100$  ppm here).

To propose a better idea of the uncertainty of CRDS data, JSR temperature evolutions of the mole fraction of  $H_2O$ ,  $CH_2O$ , and  $C_2H_4$  measured by cw-CRDS during the oxidation of *n*-heptane and *n*-decane are shown in Figure 3 for stoichiometric conditions. These profiles are compared with GC measurements and, in the case of *n*-heptane, with SVUV-PIMS profiles.<sup>3</sup> The agreement between cw-CRDS and GC is good for ethylene measured with both fuels. In the case of *n*-heptane, a good agreement for water is also seen between cw-CRDS and SVUV-PIMS. In contrast, a greater deviation between GC and CRDS measurements is observed for formaldehyde. This was also indicated by Bahrini et al.<sup>7</sup> and is due to inaccuracy in the GC measurements with the formaldehyde peak presenting a very long tail. The deviation observed between CRDS and SVUV-PIMS  $CH_2O$

measurements is due to uncertainties in cross sections used for SVUV-PIMS analysis, which shows major variations at the energy used in this study (11 eV).<sup>34</sup>

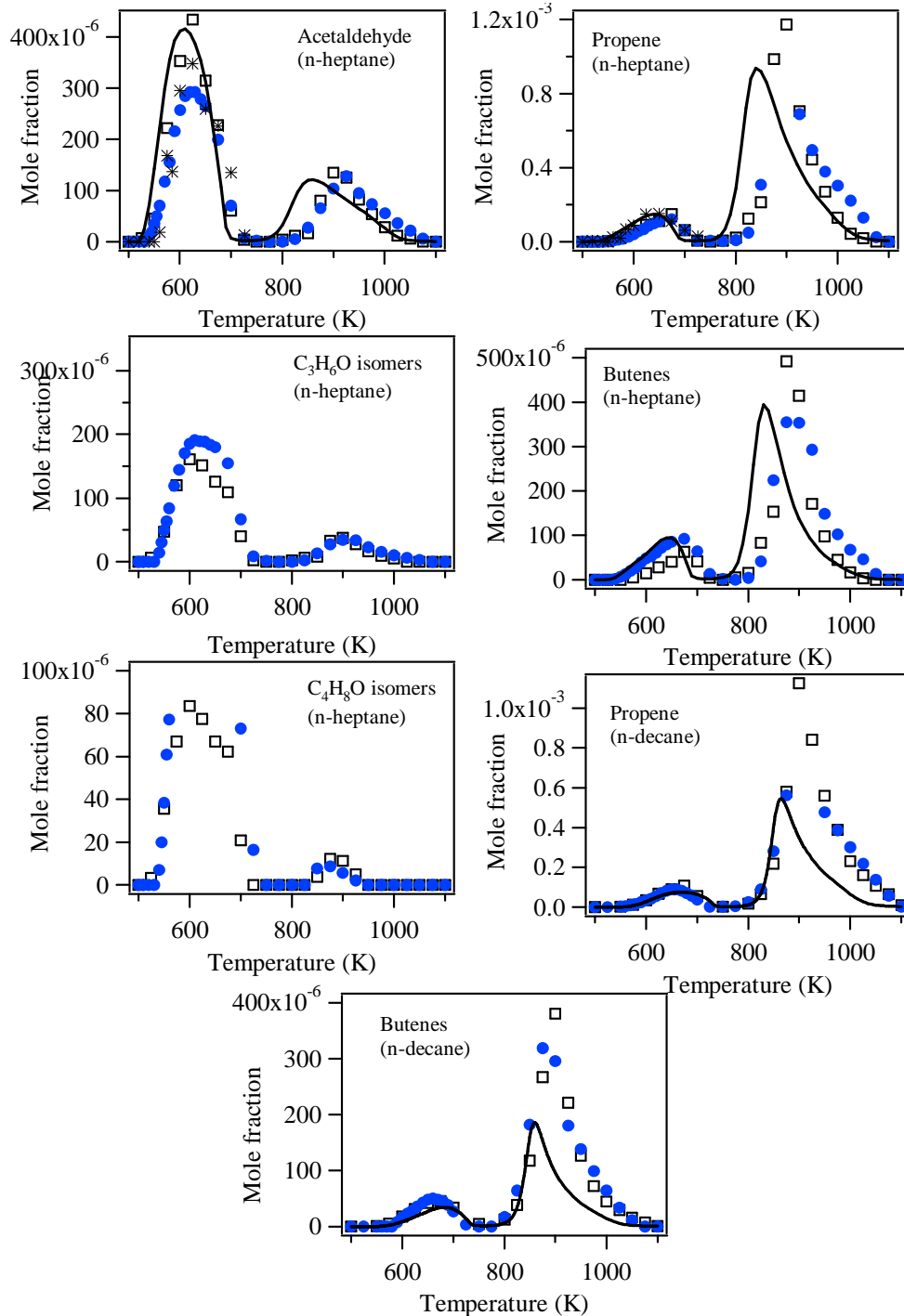


Figure 2. Temperature profiles of the mole fraction of propene, butenes, acetaldehyde,  $C_3H_6O$  isomers, and  $C_4H_8O$  isomers measured by the SPI-MS technique (blue ●, present work), by GC<sup>16</sup> (□), and by SVUV-PIMS<sup>3</sup> (\*) during *n*-heptane and *n*-decane oxidation (only present work) under stoichiometric conditions. Symbols are experiments, and lines are simulations.



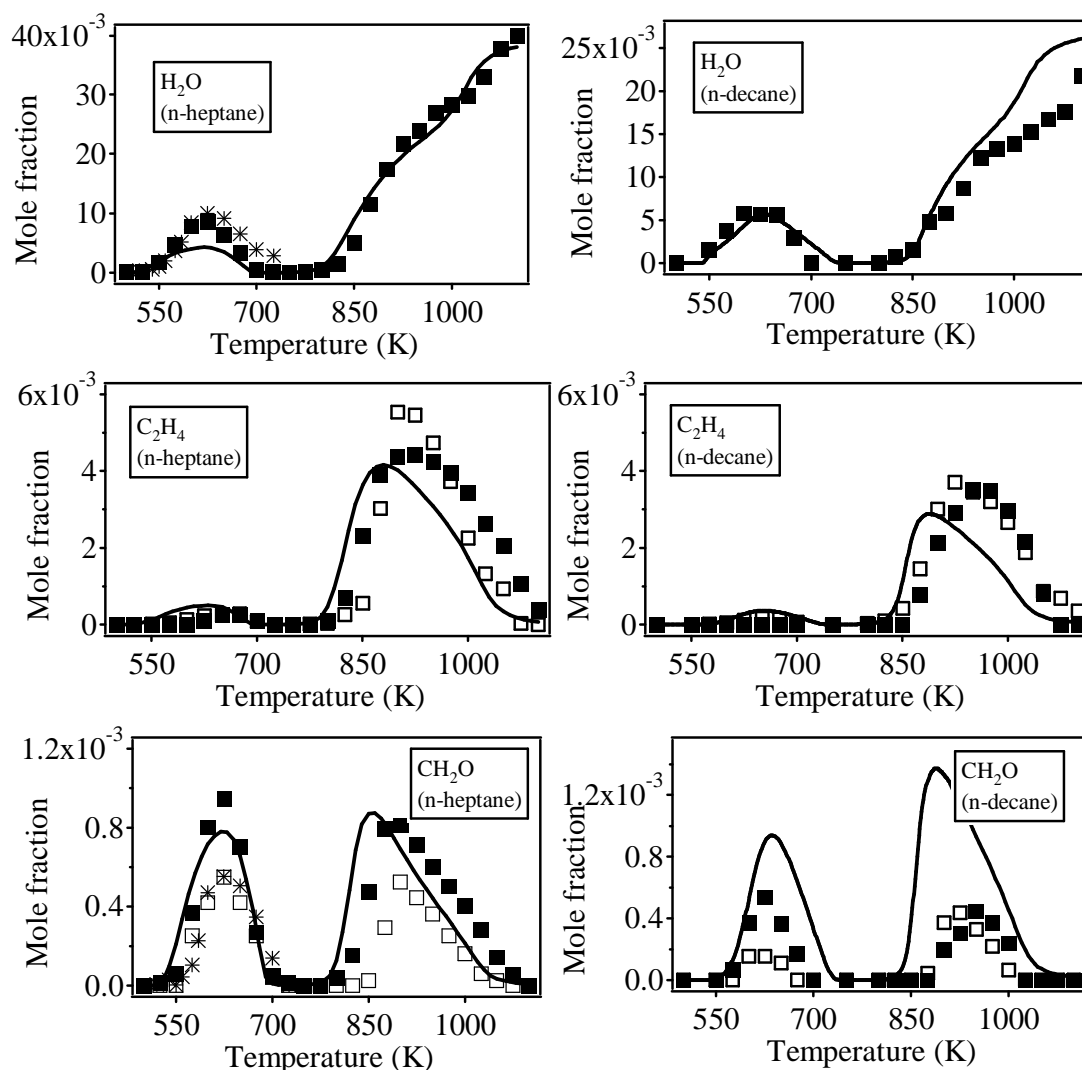


Figure 3. Temperature profiles of the mole fraction of  $\text{H}_2\text{O}$ ,  $\text{C}_2\text{H}_4$ , and  $\text{CH}_2\text{O}$  obtained during stoichiometric *n*-heptane and *n*-decane (only present work) oxidation. (■) CRDS measurements (present work). (□) GC measurements.<sup>16</sup> (\*) SVUV-PIMS.<sup>3</sup> Symbols are experiments, and lines are simulations.

### ***Ionization Energy and Thermochemical Data Calculation***

The zero-point-energy-corrected adiabatic ionization energies were calculated using the composite CBS-QB3 method<sup>35</sup> and Gaussian software<sup>36</sup> as previously described.<sup>37</sup> To attempt to reach the minimum ionization energy, the calculation was made for a representative sample of conformers. For *m/z* values equal to and above 158, the ionization energy calculations start to be very difficult due to (i) extremely long calculation times, (ii) a sharp increase of the number of conformers making it difficult to find the conformer with the lowest energy, and (iii) a decrease in calculation accuracy with the increase of carbon numbers.

When needed, theoretical calculations of thermochemical parameters were performed as described previously.<sup>37</sup> Frequencies and standard entropies were computed at the CBS-QB3 theory level. The internal degrees of freedom were treated as rigid rotor harmonic oscillators, except for the internal rotations. In this last case, hindered rotor treatment was applied. Standard enthalpies of formation were calculated by the atomization method,<sup>38</sup> whereas the enthalpies of reactions were calculated at CBS-QB3.

## Experimental Results

Below, we demonstrate how organic hydroperoxides were identified and quantified from mass spectrometry measurements. Then we present the quantification of H<sub>2</sub>O<sub>2</sub> using cw-CRDS experiments. Finally, using SPI-MS measurements, we show the quantification of ketenes and diones that are likely to be derived from organic hydroperoxides.

### Organic Hydroperoxide Identification

Figure 4 shows the laser single-photon-ionization time-of-flight mass spectra that were obtained during *n*-heptane oxidation at 600 and 850 K, respectively. Here, we will focus on peroxides and related species. The *m/z* of the major combustion products, such as those shown in Figure 2, have already been thoroughly discussed.<sup>3</sup> Their further study in this work and in our recent analysis pertaining to *n*-pentane<sup>11</sup> presents more evidence to support the hypothesis that the intermediates discussed could be peroxides.

The only organic peroxides mentioned by Herbinet et al.<sup>3</sup> (using SVUV-PIMS) were the C<sub>7</sub>-ketohydroperoxides at the *m/z* value of 146. This product can also be clearly seen in Figure 4a at a reaction temperature of 600 K. In addition, this figure presents eight other peaks not identified<sup>3</sup> as hydroperoxides, although some of them may correspond to hydroperoxides.

- *m/z* = 48: this *m/z* number could only correspond to methylhydroperoxide and had already been observed upon mass spectrometry analyses during the oxidation of *n*-butane<sup>2</sup> and *n*-pentane.<sup>11</sup> It was identified as being methylhydroperoxide (CH<sub>3</sub>OOH) from ionization energy measurements using SVUV-PIMS<sup>2,3</sup>
- *m/z* = 62: this *m/z* value was previously obtained during mass spectrometry analyses of *n*-butane<sup>2</sup> and *n*-pentane<sup>11</sup> oxidation and was identified as ethylhydroperoxide (C<sub>2</sub>H<sub>5</sub>OOH) from ionization energy measurement.
- *m/z* = 74: this *m/z* number was identified to be propanoic acid.<sup>3</sup> In this paper, we further checked for other possible isomers with this *m/z* value. Although the signal for the energy scan of this *m/z* in Figure 5a is scattered, it appears that a contribution to this *m/z* has an ionization energy close to 9.5 eV (Figure 5a). This might correspond to allyhydroperoxide (C<sub>3</sub>H<sub>5</sub>OOH). The species with *m/z* = 74 was also identified as allyhydroperoxide during *n*-pentane oxidation using the same MS apparatuses.<sup>11</sup>

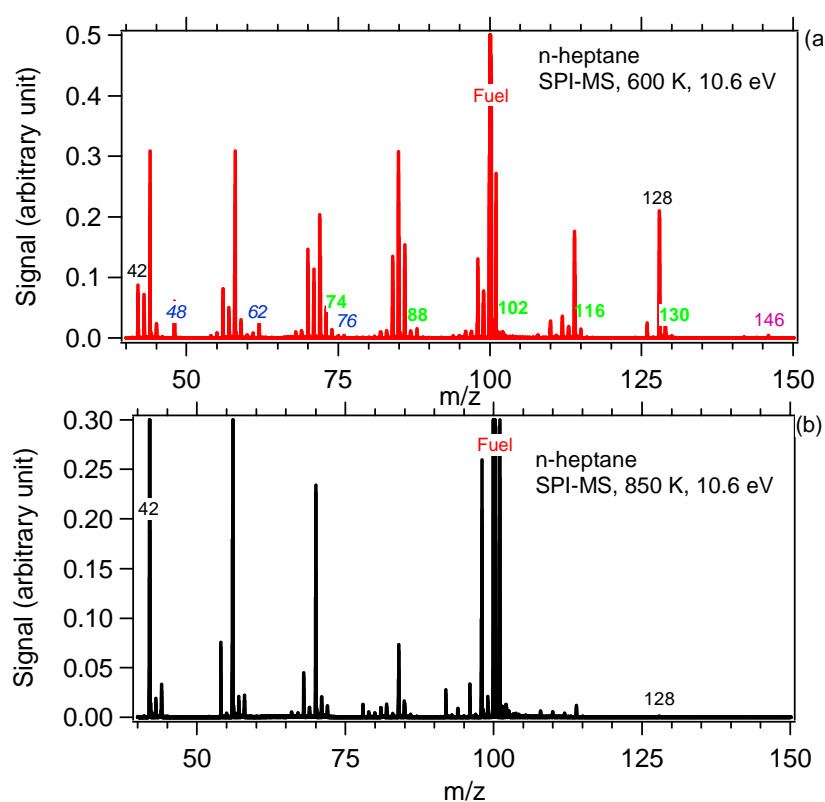


Figure 4. Mass spectra obtained during stoichiometric *n*-heptane oxidation at (a) 600 and (b) 850 K using the SPI-MS technique. The labeled *m/z* are discussed in the text: (*italic blue*) alkylhydroperoxides, (**bold green**) alkenylhydroperoxides, (*magenta*) ketohydroperoxides, and (**black**) ketene and diones.

- *m/z* = 76: this *m/z* number has not been reported during SVUV-PIMS analyses upon alkane oxidation,<sup>1</sup> but the value could correspond to propylhydroperoxide (C<sub>3</sub>H<sub>7</sub>OOH). The fact that no peak at this *m/z* number was present using SVUV-PIMS probably reflects a low sensitivity of the mass spectrometer.
- *m/z* = 88 and =102: these *m/z* values were also obtained during *n*-pentane oxidation<sup>11</sup> and were identified as being isomers of butenylhydroperoxide (C<sub>4</sub>H<sub>7</sub>OOH) and pentenylhydroperoxide (C<sub>5</sub>H<sub>9</sub>OOH), respectively. For *m/z* = 102, two peaks can be separated by SPI-MS, one corresponding to nonoxygenated compounds, most probably minor isotopes of fuel at *m/z* = 100, and one to oxygenated species.
- *m/z* = 116: this *m/z* number has not been reported during mass spectrometry analyses of alkane oxidation,<sup>1</sup> but it could correspond to isomers of hexenylhydroperoxide (C<sub>6</sub>H<sub>11</sub>OOH), as will be seen further in the text in the case of *n*-decane oxidation. Indeed, this *m/z* value was also actually detected during *n*-decane oxidation.

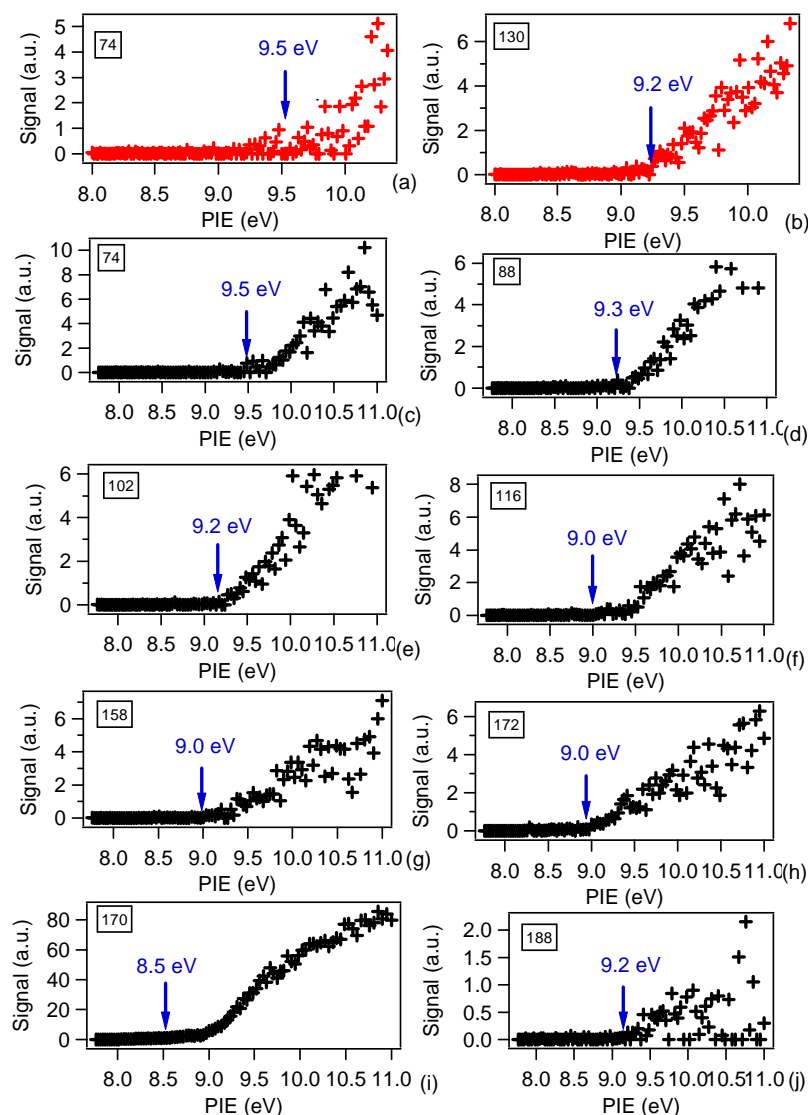
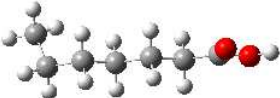
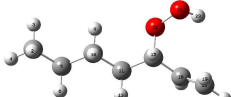
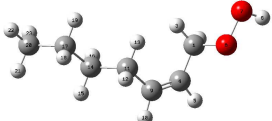
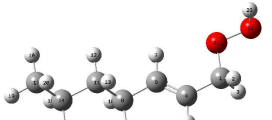

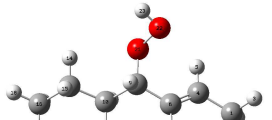
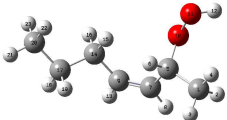



Figure 5. PIE spectra at  $m/z$  74 (a) and 130 (b) during stoichiometric *n*-heptane oxidation at 660 K<sup>3</sup> and  $m/z$  74 (c),  $m/z$  88 (d),  $m/z$  102 (e),  $m/z$  116 (f),  $m/z$  158 (g),  $m/z$  172 (h),  $m/z$  170 (i), and  $m/z$  188 (j) during stoichiometric *n*-decane (initial fuel mole fraction = 0.04) oxidation at 660 K recorded using SVUV-PIMS.

- $m/z = 130$ : this  $m/z$  value was not mentioned by ref 3 previously. The experimental measures of photon energies of this  $m/z$  by SVUV-PIMS (see Figure 5b) indicate that the signal starts to rise close to 9.2 eV. As indicated in Table 2, this value is in good agreement with calculated ionization energies for some heptenyhydroperoxide isomers ( $C_7H_{13}OOH$ ). For this  $m/z$  number, the formation of other  $C_7$  species (i.e., with the same carbon atom number as the fuel) is also possible. These include a ketone and an alcohol, which could be derived from  $C_7$  ketohydroperoxide decomposition. The ionization energies calculated for the most expected  $C_7$  isomer species, again including a ketone and an alcohol (see values in Supporting Information), cannot rule out this hypothesis.

Table 2. Calculated IE (eV) of the Most Expected Isomers Derived from *n*-Heptane at *m/z* 130

Molecule	3D structure	Calculated EI (eV)
heptanoic acid		10.14
hept-1-enyl-3-OOH		9.24
cis-hept-2-enyl-1-OOH		9.19
trans-hept-2-enyl-1-OOH		9.05
cis-hept-2-enyl-4-OOH		9.10
trans-hept-2-enyl-4-OOH		8.88
cis-hept-3-enyl-2-OOH		9.02
trans-hept-3-enyl-2-OOH		8.83

As shown in Figure 4b, these peaks all disappear at a reaction temperature of 850 K, confirming that the  $m/z$  values are related to low-temperature oxidation products.

Furthermore, two other peaks are observed in the mass spectra at 600 and 850 K of Figure 4a,b. These are likely to be derived from hydroperoxides:

- $m/z = 42$ : as shown for *n*-pentane,<sup>11</sup> this peak corresponds to a mixture of ketene ( $m/z = 42.0367$ ) and propene ( $m/z = 42.0797$ ). The two peaks can be resolved in SPI-MS experiments, whereas this was not feasible in SVUV-PIMS experiments.<sup>3</sup>
- $m/z = 128$ : this major peak at a reaction temperature of 600 K corresponds to the molar mass of  $C_7$  molecules including two carbonyl groups, which have already been clearly identified by gas chromatography.<sup>3</sup>

Figure 6 presents the mass spectra for *n*-decane oxidation at 600 K obtained using SPI-MS (initial fuel mole fraction of 0.0025) and SVUV-PIMS (initial fuel mole fraction of 0.004) experiments, respectively. The peaks corresponding to  $C_1$ - $C_3$  alkylhydroperoxides ( $m/z = 48, 62, \text{ and } 74$ ) can be observed by the SPI-MS approach (Figure 6a), but  $m/z = 62$  and  $74$  are not observed in the SVUV-PIMS experiment (Figure 6b). The  $m/z$  numbers corresponding to  $C_3$ - $C_6$  and  $C_9$ - $C_{10}$  alkenylhydroperoxides ( $m/z = 74, 88, 102, 116, 158, \text{ and } 172$ ) are present in the spectra obtained by both techniques. In contrast, the peak at  $m/z = 188$  corresponding to  $C_{10}$  ketohydroperoxide isomers is only present in the SVUV-PIMS experiment (Figure 6b), which was obtained with a highly concentrated mixture. Two high-intensity peaks corresponding to ketene/propene ( $m/z = 42$ ) and to  $C_{10}$  molecules with two carbonyl groups ( $C_{10}$  diones,  $m/z = 170$ ) were also observed. The plots of the experimental analysis of photon energies from 7.8 to 11 eV using SVUV-PIMS for  $m/z$  equal to 74, 88, 102, 116, 158, 170, 172, and 188 upon *n*-decane oxidation are shown in Figure 5c-j. The inlet fuel mole fraction is 0.004, and the temperature is 600 K.

According to the ionization energies proposed by Rodriguez et al.,<sup>11</sup> the products at  $m/z$  74, 88, and 102 are  $C_3$ - $C_5$  alkenylhydroperoxides. Although this was not considered in ref 11,  $m/z = 88$  could also correspond to  $C_3H_5OOCH_3$  isomers. However, the calculated ionization energies for the  $C_3H_5OOCH_3$  isomers suggest energies of below 9 eV (see values in Supporting Information), which are lower than the measured photoionization efficiency (PIE) onset at 9.3 eV for this  $m/z$  (see Figure 5d).

Calculated adiabatic ionization energies of the most expected isomers deriving from *n*-decane oxidation at  $m/z = 116$  are detailed in Table 3. Figure 5f shows that the signal rises at  $\sim 9.0$  eV, which is close to the IE values calculated for several hexenylhydroperoxide isomers.

The ionization energy onset for  $m/z = 158$  and  $172$ , for which ionization energy calculations were not performed, are shown in Figure 5g,h, respectively, and are just around 9 eV. If the trend showing an asymptotic decrease of the IE with the size of the alkenylhydroperoxide is expected, for example, from  $m/z$  74 (IE: 9.5 eV) to  $m/z$  130 (IE: 9.2 eV), the IEs for  $m/z$  158 and 172 might correspond to nonenylhydroperoxides and decenylhydroperoxides. For this last case, the formation of  $C_{10}$  species including a ketone and an alcohol function is also possible.

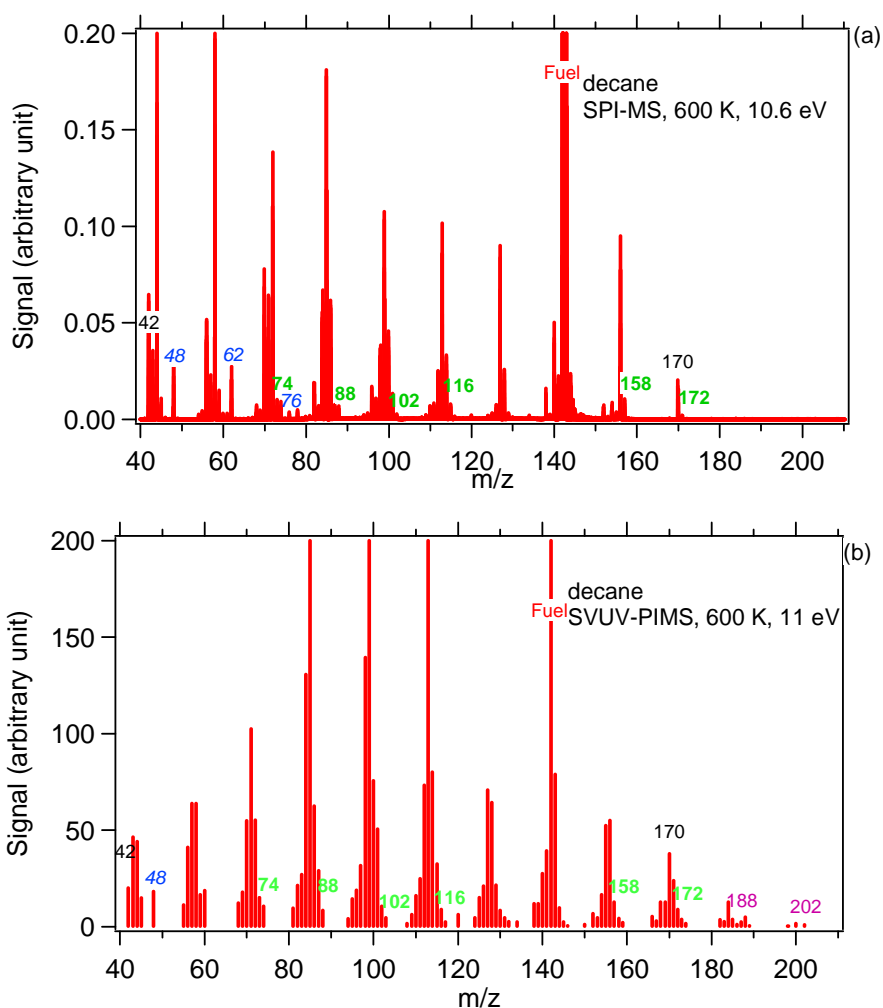


Figure 6. Mass spectra obtained during stoichiometric *n*-decane oxidation at 600 K using (a) SPI-MS and (b) SVUV-PIMS. The labeled *m/z* are discussed in the text: (*italic blue*) alkylhydroperoxides, (**bold green**) alkenylhydroperoxides, (*magenta*) ketohydroperoxides and species deriving from the third O<sub>2</sub> addition pathway, and (*black*) ketene and diones.

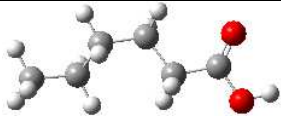
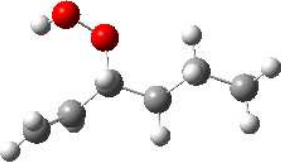
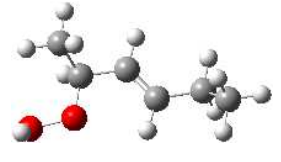
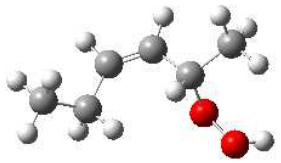
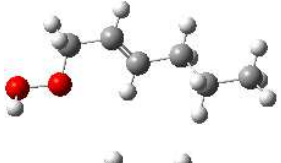
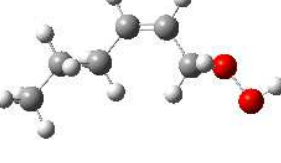


For *m/z* = 170, the profile of its PIE spectra (Figure 5i) and the signal rising from 8.5 eV are very similar to that which had been attributed to heptadiones (*m/z* = 128) in heptane oxidation by Herbinet et al.<sup>3</sup> (see comparison of the two spectra in Figure S3 of Supporting Information). Together with the fact that it corresponds to a high intensity signal, this might support the identification of *m/z* 170 as decadiones.

Figure 5j presents the PIE spectra of *m/z* = 188. Although the signal becomes more highly scattered as energy increases, a clear rise of the photoionization signal is observed at an energy of 9.2 eV. This is quite similar to what had been previously observed for C<sub>7</sub> ketohydroperoxides during *n*-heptane oxidation.<sup>3</sup> This supports that C<sub>10</sub> ketohydroperoxides are formed during *n*-decane oxidation.

Concerning the possible identification of C<sub>7</sub> and C<sub>10</sub> alkenylhydroperoxides during the oxidation of *n*-heptane and *n*-decane, respectively, it should be pointed out that a mass peak with an *m/z* value

corresponding to C<sub>7</sub> and C<sub>8</sub> alkenylhydroperoxides has been described during the JSR 2-methylhexane and 2,5-dimethylhexane oxidation followed by SVUV-PIMS at the Advanced Light Source by Wang et al.<sup>5,6</sup>

Table 3. Calculated IE (eV) of the Most Expected Isomers Derived from *n*-Decane at m/z 116

Molecule	3D structure	Calculated EI (eV)
hexanoic acid		10.21
hex-1-enyl-3-OOH		9.26
hex-3-enyl-2-OOH (trans)		8.89
hex-3-enyl-2-OOH (cis)		9.19
hex-2-enyl-1-OOH (trans)		9.12
hex-2-enyl-1-OOH (cis)		9.19
hex-2-enyl-4-OOH (trans)		8.97
hex-2-enyl-4-OOH (cis)		8.83



Note that, in the SVUV-PIMS spectrum obtained during *n*-decane oxidation with a more concentrated mixture (Figure 6b), a peak at  $m/z = 202$  is present. This  $m/z$  number might correspond to a product with a formula of  $C_{10}H_{18}O_4$ , which could be obtained through a third oxygen addition pathway as proposed by Wang et al.<sup>5</sup>

### Organic Hydroperoxide Mole Fractions as a Function of Temperature

In this section, we will discuss the quantification of the products identified in this work. For the quantification of hydroperoxides and diones, only the global mole fractions are obtained by assuming that all isomers have the same cross sections. However, an alkenylhydroperoxide has a higher PICS value than that of an alkylhydroperoxide of the same size. This is because the contribution of a C=C atom pair is some 15 times larger than that of a C-C atom pair in the energy range of 10.6–11.0 eV.

Figure 7 shows estimated mole fractions for all the organic hydroperoxides quantified by the SPI-MS method used for the oxidation of *n*-heptane and *n*-decane under stoichiometric conditions as a function of temperature.

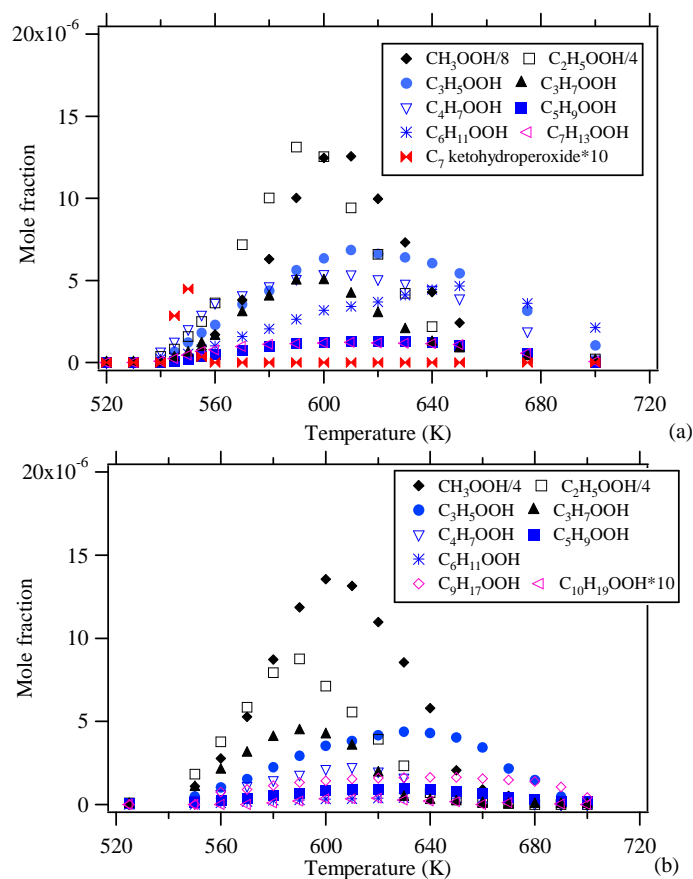


Figure 7. Temperature profiles of the mole fraction of all the organic hydroperoxides detected by SPI-MS during (a) *n*-heptane and (b) *n*-decane oxidation under stoichiometric conditions.

To scale the mole fractions of C<sub>7</sub> ketohydroperoxides and decenylhydroperoxides on the same graph as the other compounds, the former must be multiplied by a factor of 10. This led us to suspect problems in the capillary transfer line for the heavy compounds that significantly alter their quantification. This is supported for C<sub>7</sub> ketohydroperoxides by comparing the mole fractions obtained from SVUV-PIMS experiments, as shown in Figure 8a.

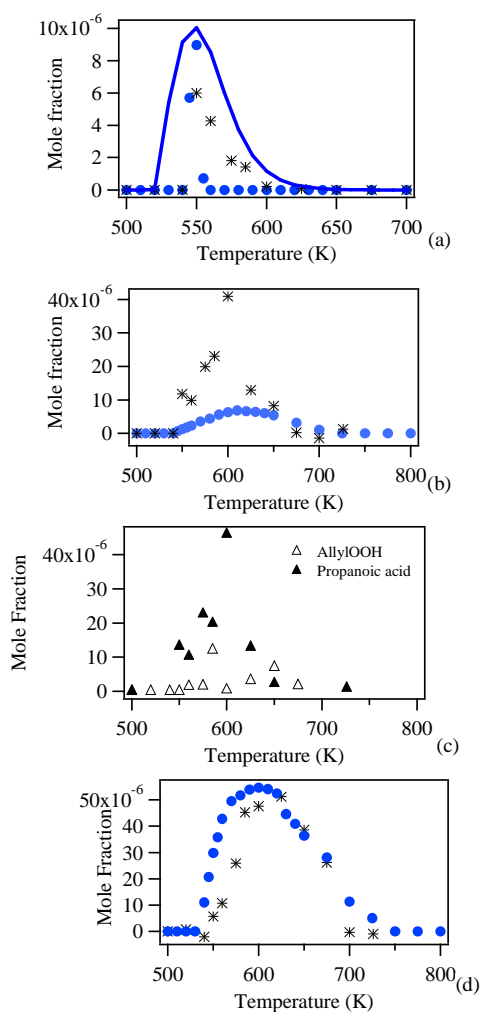


Figure 8. Temperature profiles of the mole fraction of (a) ketohydroperoxides, (b) the sum of the species obtained at  $m/z = 74$ , and (d) diones ( $m/z = 128$ ), obtained by SPI-MS (blue ●, photon energy = 10.6 eV, ketohydroperoxide mole fraction multiplied by 20) and SVUV-PIMS (\*, photon energy = 9.5 eV (a, d) and 11 eV (b)) during *n*-heptane oxidation. (a) The blue line corresponds to simulation, and the model values are divided by 75. (c) The quantified mole fraction of allylhydroperoxide and propanoic acid in SVUV-PIMS analysis of *n*-heptane oxidation.

The mole fractions obtained from SPI-MS experiments are lower than those derived from SVUV-PIMS measurements by a factor of ~20. The uncertainty in the SVUV-PIMS mole fractions of C<sub>7</sub> ketohydroperoxides is likely to be large because of the quantification method used: the signals are recorded at 9.5 eV and have typical profile shapes of hydroperoxides with a sharp peak. However,

since no reference signal is available at 9.5 eV, the used references are then the signal and corresponding mole fraction of the C<sub>7</sub> ketohydroperoxides at 550 K and 10.5 eV (with the mole fraction calculated using propene as a reference). Although a large discrepancy is observed for the quantification of C<sub>7</sub> ketohydroperoxide, the temperature at which the maximum mole fraction of these species can be observed is the same (i.e., 550 K) for both MS methods.

Figure 8b shows the variation of the estimated mole fractions of allylhydroperoxide measured by SPI-MS at 10.6 eV with temperature. At this energy, the contribution of propanoic acid (IE: 10.5 eV) should be low given the value of the cross section in ref 3. This figure also shows the measurements made by the SVUV-PIMS method at 11 eV reported to be propanoic acid.<sup>3</sup> This mole fraction corresponds to the sum of the mole fractions of allylhydroperoxide and propanoic acid. As the same measurement is available at 10 eV, it was possible to deconvolute the mole fraction of the two species, as shown in Figure 8c. Although the quantified mole fraction of allylhydroperoxide by the SVUV-PIMS method gives a scattered distribution, the maximum mole fraction is close to that obtained in the SPI-MS analysis. This confirms that the SPI-MS signal corresponds mainly to allylhydroperoxide.

### ***Alkylhydroperoxides***

Figure 9 demonstrates the species yields as a function of temperature for the three quantified alkyl hydroperoxides at four equivalence ratios in the case of *n*-heptane oxidation ( $\phi = 0.25, 1, 2, \text{ and } 4$ ). Figures 7 and 9 show that the mole fraction profiles obtained for both fuels display a single sharp maximum; at 600 K for methylhydroperoxide and at 590 K for ethylhydroperoxide and propylhydroperoxide. The temperature at which this maximum occurs does not vary with  $\phi$ . The most abundant of this type of species is methylhydroperoxide with mole fractions up to 150 ppm at  $\phi = 0.25$  for *n*-heptane, followed by ethylhydroperoxide with maximum mole fractions up to 70 ppm at  $\phi = 0.25$  for *n*-heptane. The maximum mole fractions of propylhydroperoxides are significantly lower, for example, only 5 ppm at  $\phi = 0.25$  for *n*-heptane.

The methylhydroperoxide/ethylhydroperoxide mole fraction ratio for stoichiometric mixtures is  $\sim 2$  for *n*-heptane and 1.5 for *n*-decane, while this ratio is approximately a factor of 3 during *n*-pentane JSR oxidation.<sup>11</sup> The methylhydroperoxide/propylhydroperoxide mole fraction ratio for stoichiometric mixtures is  $\sim 36$  for *n*-heptane and 10 for *n*-decane. This is consistent with the fact that larger molecules produce more C<sub>2</sub>-C<sub>3</sub> alkyl radicals through  $\beta$ -scission decomposition.

Figure 9 shows that, for a given temperature, the mole fraction of methylhydroperoxide gradually increases when  $\phi$  decreases. This is also the case for ethylhydroperoxide. The mole fractions of propylhydroperoxides remain quasi constant for  $\phi$  values from 0.25 to 2. For the three alkylhydroperoxides, the mole fractions observed are significantly lower at  $\phi = 4$  than at  $\phi = 2$ .

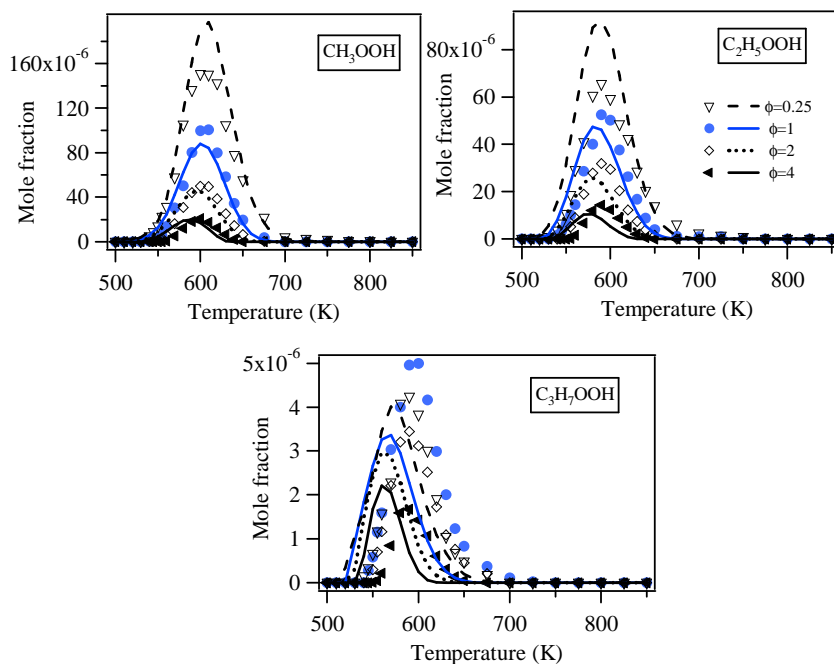


Figure 9. Temperature profiles of the mole fraction of all alkylhydroperoxides obtained by SPI-MS during *n*-heptane oxidation for various equivalence ratios. Symbols are experiments, and lines are simulations (model values divided by 3, 5, and 2, for  $\text{CH}_3\text{OOH}$ ,  $\text{C}_2\text{H}_5\text{OOH}$ , and  $\text{C}_3\text{H}_7\text{OOH}$ , respectively).

### Alkenylhydroperoxides

Figure 10 shows the evolution of the estimated mole fractions for the quantified  $\text{C}_3$ – $\text{C}_7$  alkenyl hydroperoxides for four equivalence ratios in the case of *n*-heptane oxidation ( $\phi = 0.25, 1, 2,$  and  $4$ ) as a function of temperature. Figures 7 and 10 demonstrate that the mole fraction profiles obtained for the two fuels display a single sharp maximum. In addition, these maxima occur at slightly higher temperatures than those for alkylhydroperoxides, except for butenylhydroperoxides measured in rich and stoichiometric mixtures. However, as shown in Figure 10, the most striking difference between alkenylhydroperoxide and alkylhydroperoxide profiles is that in the former case the temperature of the maximum mole fraction at  $\phi = 0.25$  is  $\sim 40$  K higher than that for rich and stoichiometric mixtures. For these alkenylhydroperoxides, the most abundant species is allylhydroperoxide, which has mole fractions up to 13 ppm at  $\phi = 0.25$ . This is followed by butenylhydroperoxides and hexenylhydroperoxides with maximum mole fractions up to 5 ppm at  $\phi = 1$ . The maximum mole fractions of  $\text{C}_5$  and  $\text{C}_7$  species are significantly lower, being only 1.2 ppm at  $\phi = 1$ . Figure 10 shows that, for a given temperature above 600 K, the mole fraction of allylhydroperoxide gradually increases when  $\phi$  decreases, with a sharp increase at  $\phi = 0.25$ . The situation is different for the other compounds, where the mole fraction gradually increases when  $\phi$  decreases for rich and stoichiometric mixtures, but where the mole fraction at  $\phi = 0.25$  is lower than those at  $\phi = 1.0$ .

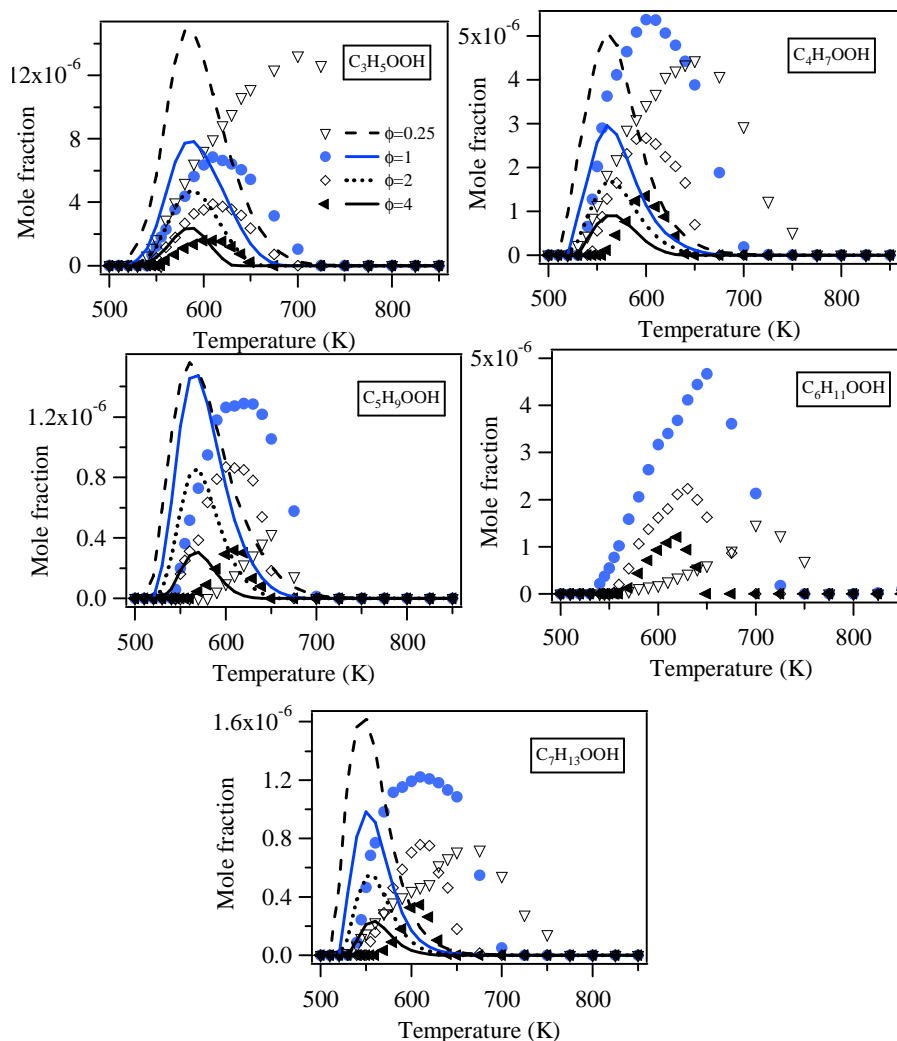


Figure 10. Temperature profiles of the mole fraction of all the alkenylhydroperoxides obtained by SPI-MS during *n*-heptane oxidation for various equivalence ratios. Symbols are experiments, and lines are simulations (model values multiplied by 3, 5, and 40, for  $C_3H_5OOH$ ,  $C_4H_7OOH$ , and  $C_5H_9OOH$ , respectively; model values divided by 50 for  $C_7H_{13}OOH$ ).

### ***Evolution of $H_2O_2$ Mole Fractions as a Function of Temperature***

The evolution of the mole fraction of  $H_2O_2$  during the oxidation of *n*-heptane as a function of temperature is shown in Figure 11. Measurements at  $\phi = 1$  were made using CRDS, but also SVUV-PIMS experiments were made at a photon energy of 13.05 eV. The PICS at this energy has been extrapolated from the measurements of Dodson et al.<sup>21</sup> A good agreement is found between the two types of measurement confirming the reliability of CRDS measurements for fuels as large as *n*-heptane. A similar good agreement was seen between CRDS and SVUV-PIMS  $H_2O_2$  measurements in our previous study of *n*-pentane oxidation.<sup>11</sup>

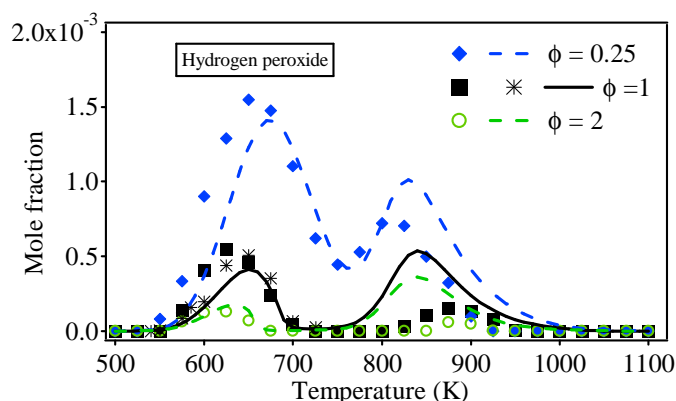


Figure 11. Temperature profiles of the mole fraction of  $\text{H}_2\text{O}_2$  obtained during  $n$ -heptane oxidation for various equivalence ratios. Symbols are experiments, and lines are simulations. ( $\circ$ ,  $\blacksquare$ ,  $\blacklozenge$ ) CRDS measurements and ( $*$ ) SVUV-PIMS measurements at a photon energy of 13.05 eV.

To our knowledge, these experiments with  $n$ -heptane are the first  $\text{H}_2\text{O}_2$  quantifications in JSR oxidation studies using CRDS with such a large fuel molecule. This quantification was not possible in the case of  $n$ -decane oxidation due to condensation at the inlet of the cell. Condensation problems increase the background noise, which affects  $\text{H}_2\text{O}_2$  measurement more than that of other products due to its low signal intensity, which is close to the detection limit.

In the case of  $n$ -heptane, quantification was also possible for  $\phi$  values of 0.25, 1, and 2, but not for  $\phi = 4$ , where the formation was too low. Figure 11 shows that the mole fraction profiles obtained display two maxima: a first one at temperatures below 650 K and a second one around 850 K. The results show a significant influence of equivalence ratio, with the maximum value at  $\phi = 0.25$ , being  $\sim 7$  times higher than that at  $\phi = 2$ . The equivalence ratio also has an influence on the temperatures at which these maxima are observed.

### ***Ketene and Dione Mole Fractions as a Function of Temperature***

Figure 8d displays the estimated mole fractions of diones with the same carbon number as the fuel measured by SVUV-PIMS and SPI-MS methods during  $n$ -heptane oxidation under stoichiometric conditions, according to the temperature. A good agreement between the two profiles was seen.

Figure 12 presents the temperature evolution of the estimated mole fractions of diones with the same carbon number as the fuel and ketene obtained by SPI-MS during  $n$ -heptane oxidation for various equivalence ratios. Furthermore, it shows  $n$ -decane oxidation under stoichiometric conditions. For both fuels, the ketene mole fraction profiles exhibit two peaks. The temperature at which the low-temperature maximum is observed and the values of the mole fraction reached increases when  $\phi$  decreases, whereas for the high-temperature maximum the opposite is seen. At low temperatures, the formation of ketene is favored when  $\phi$  decreases.

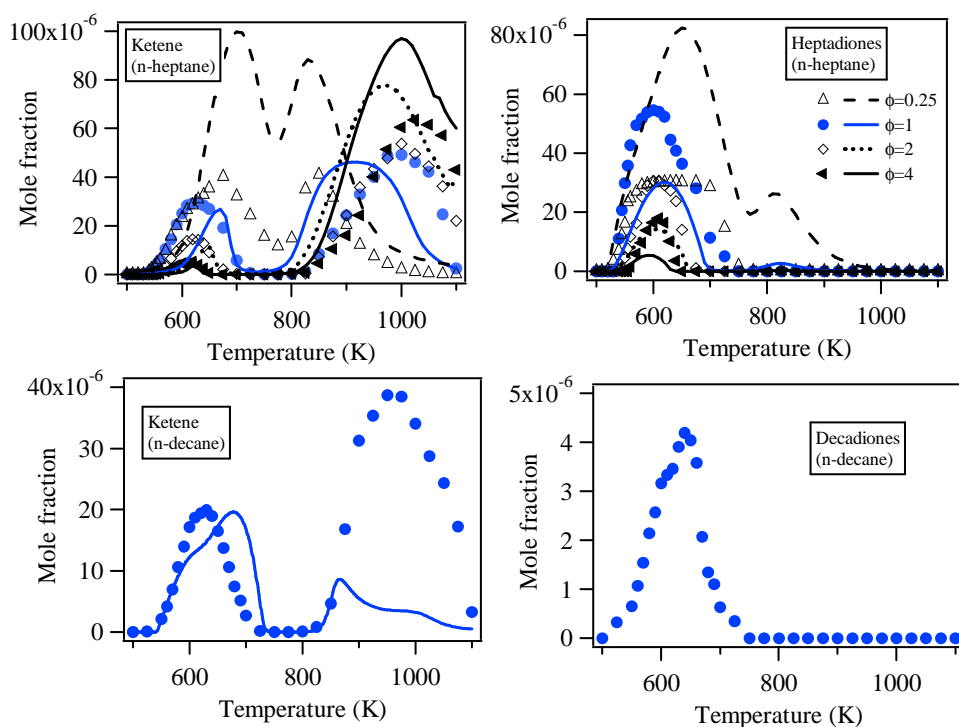


Figure 12. Temperature profiles of the mole fraction of all the diones and ketene obtained by SPI-MS during *n*-heptane oxidation for various equivalence ratios and *n*-decane oxidation under stoichiometric conditions. Symbols are experiments, and lines are simulations (model values divided by 10 for ketene (*n*-decane) and multiplied by 50 for heptadiones (*n*-heptane)).

For both fuels, the dione mole fraction profiles exhibit a single peak at  $\sim 600$  K. For *n*-heptane, at  $\phi$  equal to 0.25, a plateau from 600 to 650 K exists. At a given temperature, the largest mole fraction of heptadiones is obtained for  $\phi = 1$  (e.g.,  $\sim 55$  ppm). At a given temperature, the mole fractions of decadiones are  $\sim 10$  times lower than those of heptadiones. This could be due to transfer problems in the capillary line.

## Discussion

To analyze more thoroughly experimental results described previously, we performed simulations using two up-to-date models described previously. These models have been partially validated by JSR results obtained in the same reactor as that used in the present study. Simulations were performed using the OpenSMOKE++ framework<sup>39</sup> for *n*-heptane and the CHEMKIN package<sup>40</sup> for *n*-decane; in both simulations, JSR was modeled as a perfectly stirred reactor.

For *n*-heptane, we used the model proposed by Zhang et al.,<sup>16</sup> which was developed from newly revised kinetic rate rules based on recent theoretical calculations.<sup>41</sup> The performance of this model can be seen in Figures 2, 3, and S1, for fuel conversion and the formation of some main reaction products (water, ethylene, formaldehyde, acetaldehyde, propene, and butenes). Globally the agreement between experimental results and simulations is satisfactory. However, as can be seen in Figure S1, while the predictions are good for rich and stoichiometric mixtures, the fuel conversion is not as well-predicted below 800 K for  $\phi = 0.25$ .

For *n*-decane, we used the model proposed by Herbinet et al.<sup>17</sup> The *n*-decane oxidation part of this model was automatically generated using the EXGAS code as described by Biet et al.<sup>42</sup> To use this model, the reactions related to aromatic compounds were removed, and the rate constant proposed by Baulch et al.<sup>43</sup> for hydroperoxide decomposition was applied. The performance of this model can be seen in Figures 2, 3, and S1, and is rather good for fuel conversion and the production of some main reaction products (water, ethylene, propene, and butenes). Overprediction of formaldehyde occurs, especially above 800 K.

These models were used to reproduce the formation of peroxides, ketene, and diones. Figures 9 and 13 show that both models predict the mole fractions of C<sub>1</sub>–C<sub>3</sub> alkyl hydroperoxides rather satisfactorily as a function of temperature, taking into account the significant uncertainty due to the estimated PICS and sampling method. The evolution of the mole fractions of C<sub>1</sub>–C<sub>2</sub> alkyl hydroperoxides with temperature is especially well-reproduced by the *n*-heptane model with a good simulation of the location of the maximum mole fraction and of the variation when varying  $\phi$ . Deviations of a few kelvin in the temperature of the maximum mole fraction can be noted when modeling C<sub>3</sub>H<sub>7</sub>OOH for *n*-heptane and C<sub>1</sub>–C<sub>2</sub> alkyl hydroperoxides for *n*-decane.

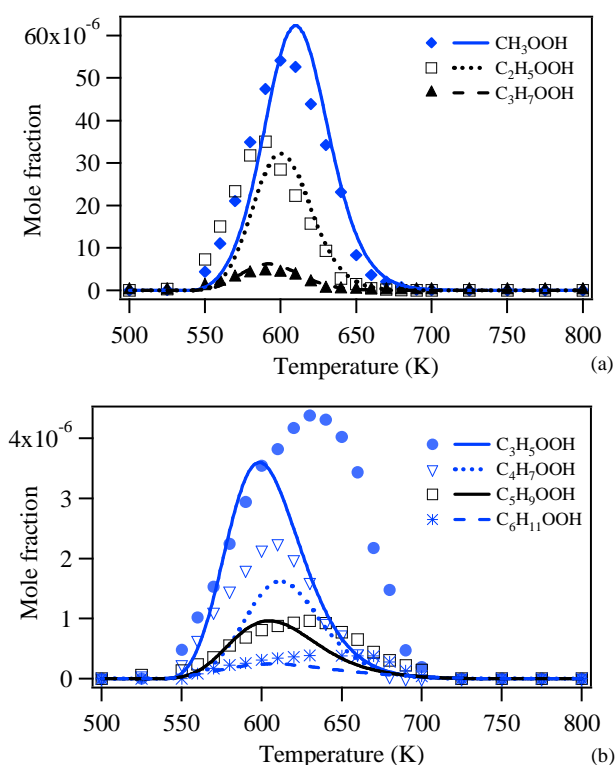


Figure 13. Temperature profiles of the mole fraction of (a) alkylhydroperoxides and (b) alkenylhydroperoxydes obtained by SPI-MS during *n*-decane oxidation under stoichiometric conditions. Symbols are experiments, and lines are simulations (model values divided by 3, 2, and 8 for CH<sub>3</sub>OOH, C<sub>2</sub>H<sub>5</sub>OOH, and C<sub>3</sub>H<sub>7</sub>OOH, respectively, and model values multiplied by 2 and 10 for C<sub>5</sub>H<sub>9</sub>OOH and C<sub>6</sub>H<sub>11</sub>OOH, respectively).



A rate analysis performed at 610 K for stoichiometric mixtures indicates that C<sub>1</sub>–C<sub>3</sub> alkyl hydroperoxides are dominantly produced from the disproportionations of C<sub>1</sub>–C<sub>3</sub> alkyl peroxy radicals with HO<sub>2</sub> radicals. The agreement between experiments and simulations shown in Figures 9 and 13 indicate that the C<sub>1</sub>–C<sub>2</sub> alkyl peroxy radical chemistry is well-understood in the recent core mechanism<sup>44</sup> used in the model of Zhang et al.<sup>16</sup> and not too badly in the older core mechanism<sup>45</sup> used by Herbinet et al.<sup>17</sup> The overestimation of C<sub>3</sub>H<sub>7</sub>OOH for *n*-decane (see Figure 13) is probably more than what could be explained by PICS uncertainty. This is most likely because of less accurate propyl chemistry in the *n*-decane model,<sup>17</sup> which only includes a C<sub>0</sub>–C<sub>2</sub> core mechanism.<sup>45</sup>

Figure 8a shows a simulated mole fraction evolution with temperature for ketohydroperoxides obtained during *n*-heptane oxidation. Although the temperature at which the maximum mole fraction occurs is well-predicted, even the SVUV-PIMS mole fraction values are overestimated by a factor of 75. The discrepancy is large even when a significant uncertainty is taken into account. This may be attributed to the decomposition or quenching of fragile ketohydroperoxides during analysis and sampling, even when probing via a molecular beam. Also, the incomplete understanding of the ketohydroperoxide degradation mechanism cannot be ruled out.

As both models consider the formation of alkenyl hydroperoxides, the experiment shown in Figure 10 was devised. This Figure presents the experimental and simulated mole fractions of C<sub>3</sub>–C<sub>5</sub> and C<sub>7</sub> alkenyl hydroperoxides obtained during *n*-heptane oxidation. Similarly, Figure 13 displays experimental and simulated mole fractions of C<sub>3</sub>–C<sub>6</sub> alkenyl hydroperoxides produced during *n*-decane oxidation. C<sub>6</sub> alkenyl hydroperoxides were also considered in the model of Zhang et al.,<sup>16</sup> but underestimation of the experimental values by a factor of ~500 is observed in our simulations. Thus, these simulations are not presented in Figure 10.

Apart from C<sub>4</sub>H<sub>7</sub>OOH in the case of *n*-decane, the temperature at which the simulated mole fraction reaches its maximum can be seen is lowered by at least 15 K for all the alkenyl hydroperoxides measured in the two fuel oxidations. Updating the thermochemical parameters by using theoretically calculated thermochemical data for C<sub>3</sub>–C<sub>5</sub> alkenyl hydroperoxide isomers (see data in Supporting Information) has no effect on the location of the temperature where the maximum mole fraction is observed. For the effect of equivalence ratio on *n*-heptane oxidation, the model predicts higher mole fraction values for  $\phi = 0.25$  for all the simulated alkenyl hydroperoxides. However, this phenomenon was only experimentally observed for C<sub>3</sub>H<sub>5</sub>OOH. Taking into account PICS estimations, the deviation obtained between experimental and predicted mole fraction values are reasonable for C<sub>3</sub>–C<sub>4</sub> alkenyl hydroperoxides in both fuel oxidation studies, as well as for C<sub>5</sub>H<sub>9</sub>OOH in the case of *n*-decane. However, the discrepancies for the other compounds are too large to be easily explained.

The rate analysis indicates that, for both fuels, C<sub>3</sub>–C<sub>4</sub> alkenylhydroperoxides are mainly produced via the combinations of resonance-stabilized alkenyl (or allylic) radicals with HO<sub>2</sub> radicals. This is also the case for C<sub>5</sub>H<sub>9</sub>OOH and C<sub>6</sub>H<sub>11</sub>OOH in the case of *n*-decane. For the rate constants of the C<sub>3</sub>H<sub>5</sub>OOH-related reactions, the *n*-heptane model uses the recent theoretically computed rate constants proposed by Goldsmith et al.,<sup>46</sup> while the *n*-decane model uses estimated values. The results show that the different rate constants for the combination of alkenyl radicals and HO<sub>2</sub> radicals have no effect on the temperature of the maximum mole fraction. With the exception of C<sub>6</sub>H<sub>11</sub>OOH in the case of *n*-decane, the order of magnitude of the maximum mole fractions of alkenylhydroperoxides is well-simulated, indicating some pertinence of the considered pathway: the combinations of resonance-

stabilized alkenyl radicals with HO<sub>2</sub> radicals. However, the deviation between simulations and experiments related to the location of the temperature corresponding to maximum mole fraction and in the equivalence ratio influence indicate that the alkenyl radical low-temperature oxidation chemistry is still not fully understood, even for allyl radicals. For example, Figure 14 shows that the temperature corresponding to the maximum mole fraction is significantly influenced by the activation energy of hydroperoxide decomposition to yield alkoxy and OH radicals. A 2 kcal/mol increase in activation energy increases this temperature value by ~15 K. The increase of the activation energy may be reasonable, since Goldsmith et al.<sup>46</sup> have reported that there was some uncertainty in their calculated barrier heights due to multireference effects.

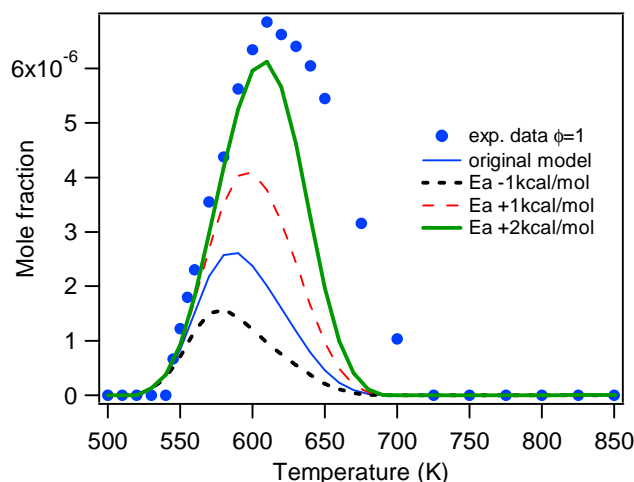


Figure 14. Influence of the activation energy of the hydroperoxide decomposition on the temperature corresponding to the maximum mole fraction of allylhydroperoxide during *n*-heptane oxidation under stoichiometric conditions.

The rate analysis shows that, for *n*-heptane, the alkenylhydroperoxides with more than five carbon atoms mainly result from the reactions of hydroperoxyalkylperoxy radicals and dihydroperoxyalkyl radicals via HO<sub>2</sub> radical elimination. These reactions were recently considered in the Galway alkane model.<sup>16</sup> The combinations of alkenyl radicals with more than five carbon atoms with HO<sub>2</sub> radicals are not taken into account in the model, which may explain why C<sub>5-6</sub> alkenylhydroperoxides are considerably underestimated. Since C<sub>7</sub> hydroperoxyalkylperoxy radicals and dihydroperoxyalkyl radicals can easily be produced from fuel reactions, the significant overprediction of C<sub>7</sub>H<sub>13</sub>OOH could indicate some problems during sampling.

The simulated results for hydrogen peroxide (for *n*-heptane) are plotted in Figure 11, showing a satisfactory agreement with the experimental results. The variations when altering  $\phi$  are well-reproduced.

The simulated results for ketene in *n*-heptane and *n*-decane oxidation, and heptadiones in *n*-heptane oxidation, are displayed in Figure 12. The simulated results for the decadiones were not shown, because their corresponding reactions were not considered in the *n*-decane model. The ketene mole fraction is satisfactorily reproduced by the *n*-heptane model for  $\phi$  from 1 to 4, but it is significantly overestimated at  $\phi = 0.25$ ; this should relate to a worse prediction of reactivity at this equivalence ratio (see Figure S1). However, the influence of  $\phi$  on the mole fraction of ketenes at both low and high

temperatures is well-reproduced by the model. In the case of *n*-decane, the model needs to be significantly improved for ketene predictions. The rate analysis indicates that, for *n*-heptane below 800 K, ketene is mainly produced from the decomposition of alkoxy radicals, which come from the decomposition of ketohydroperoxides. These pathways are favored in lean mixtures. In contrast, above 800 K, the reactions of oxygenated species (OH, O, O<sub>2</sub>) with ethylene and propene, which explains ketene formation, are promoted in rich mixtures.

While the profiles of heptadiones are accurately predicted for  $\phi$  from 1 to 4 with an enlargement of the mole fraction peak at  $\phi = 1$  and 0.25 as is experimentally observed, the actual experimental mole fraction values are underpredicted by a factor of 50. The model of Herbinet et al.,<sup>3</sup> which considered the formation of diones by ketohydroperoxide molecular decomposition and reactions of the alkoxy radicals deriving from ketohydroperoxide, encountered the same problem in their study under stoichiometric conditions. The model of Pelucchi et al.<sup>47</sup> proposes that diones are formed via H-abstractions from ketohydroperoxides by a wide range of radicals and followed by a direct decomposition of the obtained radicals. For stoichiometric conditions, this model predicts accurately the order of magnitude for the dione mole fractions, but with too narrow a peak. The model of Zhang et al.<sup>16</sup> that we used here considers the reactions proposed by both Herbinet et al.<sup>3</sup> and by Pelucchi et al.<sup>47</sup> However, this model only considers the H-abstractions from ketohydroperoxides by OH radicals, and the rate constant was reduced by a factor of 270 at 600 K. The understanding of the chemistry of the formation of these important oxidation products is still not complete.

## Conclusion

Using a jet-stirred reactor coupled to three diagnostic techniques (SVUV-PIMS, SPI-MS, and cw-CRDS), ketene, C<sub>7</sub>- and C<sub>10</sub> diones, as well as many hydroperoxides (C<sub>1</sub>-C<sub>3</sub> alkyl hydroperoxides, C<sub>3</sub>-C<sub>7</sub> alkenyl hydroperoxides, C<sub>7</sub> ketohydroperoxides, and H<sub>2</sub>O<sub>2</sub>) have been detected, and quantified in most cases, during the gas-phase oxidation of two common fuel surrogates: *n*-heptane and *n*-decane. Experimental measurements have been compared to simulations performed using up-to-date detailed kinetic models described in the literature. The results show a good understanding of H<sub>2</sub>O<sub>2</sub> and C<sub>1</sub>-C<sub>2</sub> alkyl hydroperoxide chemistry for a large range of equivalence ratios (e.g., 0.25 to 4) and a reasonable one for ketene. However, many uncertainties remain concerning the pathways for degradation of ketohydroperoxides and the reactions of alkenyl hydroperoxides, even if the importance of the combination of alkenyl and HO<sub>2</sub> radicals has been outlined. This study shows that special attention must be paid to the mechanism for unsaturated hydroperoxides, ketohydroperoxides, and diones in future model development.

## Reference

- (1) Herbinet, O.; Battin-Leclerc, F. Progress in Understanding Low-Temperature Organic Compound Oxidation Using a Jet-Stirred Reactor. *Int. J. Chem. Kinet.* 2014, 46, 619–639.
- (2) Herbinet, O.; Battin-Leclerc, F.; Bax, S.; Le Gall, H.; Glaude, P.-A.; Fournet, R.; Zhou, Z.; Deng, L.; Guo, H.; Xie, M.; et al. Detailed Product Analysis During the Low Temperature Oxidation of *n*-Butane. *Phys. Chem. Chem. Phys.* 2011, 13, 296–308.

- (3) Herbinet, O.; Husson, B.; Serinyel, Z.; Cord, M.; Warth, V.; Fournet, R.; Glaude, P.-A.; Sirjean, B.; Battin-Leclerc, F.; Wang, Z.; et al. Experimental and Modeling Investigation of the Low-Temperature Oxidation of n-Heptane. *Combust. Flame* 2012, 159, 3455–3471.
- (4) Eskola, A. J.; Welz, O.; Zádor, J.; Antonov, I. O.; Sheps, L.; Savee, J. D.; Osborn, D. L.; Taatjes, C. A. Probing the Low-Temperature Chain-Branching Mechanism of n-Butane Autoignition Chemistry via Time-Resolved Measurements of Ketohydroperoxide Formation in Photolytically Initiated n-C<sub>4</sub>H<sub>10</sub> Oxidation. *Proc. Combust. Inst.* 2015, 35, 291–298.
- (5) Wang, Z.; Zhang, L.; Moshhammer, K.; Popolan-Vaida, D. M.; Shankar, V. S. B.; Lucassen, A.; Hemken, C.; Taatjes, C. A.; Leone, S. R.; Kohse-Höinghaus, K.; et al. Additional Chain-Branching Pathways in the Low-Temperature Oxidation of Branched Alkanes. *Combust. Flame* 2016, 164, 386–396.
- (6) Wang, Z.; Mohamed, S. Y.; Zhang, L.; Moshhammer, K.; Popolan-Vaida, D. M.; Shankar, V. S. B.; Lucassen, A.; Ruwe, L.; Hansen, N.; Dagaut, P.; et al. New Insights into the Low-Temperature Oxidation of 2-Methylhexane. *Proc. Combust. Inst.* 2016, DOI: 10.1016/j.proci.2016.06.085
- (7) Bahrini, C.; Herbinet, O.; Glaude, P.-A.; Schoemaeker, C.; Fittschen, C.; Battin-Leclerc, F. Quantification of Hydrogen Peroxide during the Low-Temperature Oxidation of Alkanes. *J. Am. Chem. Soc.* 2012, 134, 11944–11947.
- (8) Bahrini, C.; Morajkar, P.; Schoemaeker, C.; Frottier, O.; Herbinet, O.; Glaude, P.-A.; Battin-Leclerc, F.; Fittschen, C. Experimental and Modeling Study of the Oxidation of n-Butane in a Jet Stirred Reactor Using cw-CRDS Measurements. *Phys. Chem. Chem. Phys.* 2013, 15, 19686–19698.
- (9) Djehiche, M.; Le Tan, N. L.; Jain, C. D.; Dayma, G.; Dagaut, P.; Chauveau, C.; Pillier, L.; Tomas, A. Quantitative Measurements of HO<sub>2</sub> and Other Products of n-Butane Oxidation (H<sub>2</sub>O<sub>2</sub>, H<sub>2</sub>O, CH<sub>2</sub>O, and C<sub>2</sub>H<sub>4</sub>) at Elevated Temperatures by Direct Coupling of a Jet-Stirred Reactor with Sampling Nozzle and Cavity Ring-Down Spectroscopy (cw-CRDS). *J. Am. Chem. Soc.* 2014, 136, 16689–16694.
- (10) Kurimoto, N.; Brumfield, B.; Yang, X.; Wada, T.; Diévert, P.; Wysocki, G.; Ju, Y. Quantitative Measurements of HO<sub>2</sub>/H<sub>2</sub>O<sub>2</sub> and Intermediate Species in Low and Intermediate Temperature Oxidation of Dimethyl Ether. *Proc. Combust. Inst.* 2015, 35, 457–464.
- (11) Rodriguez, A.; Herbinet, O.; Wang, Z.; Qi, F.; Fittschen, C.; Westmoreland, P. R.; Battin-Leclerc, F. Measuring Hydroperoxide Chain-Branching Agents During n-Pentane Low-Temperature Oxidation. *Proc. Combust. Inst.*, 2016, DOI: 10.1016/j.proci.2016.05.044.
- (12) Herbinet, O.; Dayma, G. Jet-Stirred Reactor. In *Cleaner Combustion*; Battin-Leclerc, F., Simmie, J. M., Blurock E., Eds.; Springer London, 2013; pp 183–210.
- (13) Guibet, J. C. *Fuels and engines*; Publications de l'Institut Français du Pétrole, Eds. Technip: Paris, 1999.
- (14) Zeng, M.; Yuan, W.; Wang, Y.; Zhou, W.; Zhang, L.; Qi, F.; Li, Y. Experimental and Kinetic Modeling Study of Pyrolysis and Oxidation of n-Decane. *Combust. Flame* 2014, 161, 1701–1715.
- (15) Battin-Leclerc, F. Detailed Chemical Kinetic Models for the Low-Temperature Combustion of Hydrocarbons with Application to Gasoline and Diesel Fuel Surrogates. *Prog. Energ. Combust. Sci.* 2008, 34, 440–498.
- (16) Zhang, K.; Banyon, C.; Bugler, J.; Curran, H. J.; Rodriguez, A.; Herbinet, O.; Battin-Leclerc, F.; B'Chir, C.; Heufer, K. A. An Updated Experimental and Kinetic Modeling Study of n-Heptane Oxidation. *Combust. Flame* 2016, 172, 116–135.
- (17) Herbinet, O.; Husson, B.; Ferrari, M.; Glaude, P.-A.; Battin-Leclerc, F. Low Temperature Oxidation of Benzene and Toluene in Mixture with n-Decane. *Proc. Combust. Inst.* 2013, 34, 297–305.
- (18) Qi, F. Combustion Chemistry Probed by Synchrotron VUV Photoionization Mass Spectrometry. *Proc. Combust. Inst.* 2013, 34, 33–63.

- (19) Battin-Leclerc, F.; Herbinet, O.; Glaude, P.-A.; Fournet, R.; Zhou, Z.; Deng, L.; Guo, H.; Xie, M.; Qi, F. Experimental Confirmation of the Low-Temperature Oxidation Scheme of Alkanes. *Angew. Chem. Int. Ed.* 2010, 49, 3169–3172.
- (20) Qi, F.; Yang, R.; Yang, B.; Huang, C.; Wei, L.; Wang, J.; Sheng L.; Zhang, Y. Isomeric Identification of Polycyclic Aromatic Hydrocarbons Formed in Combustion with Tunable Vacuum Ultraviolet Photoionization. *Rev. Sci. Instrum.*, 2006, 77, 084101.
- (21) Dodson, L. G.; Shen, L.; Savee, J. D.; Eddingsaas, N. C.; Welz, O.; Taatjes, C. A.; Osborn, D. L.; Sander, S. P.; Okumura, M. VUV Photoionization Cross Sections of HO<sub>2</sub>, H<sub>2</sub>O<sub>2</sub>, and H<sub>2</sub>CO. *J. Phys. Chem. A* 2015, 119, 1279–1291.
- (22) Jia, L.; Le-Brech, Y.; Shrestha, B.; Frowein, M. B.; Ehlert, S.; Mauviel, G.; Zimmermann, R.; Dufour, A. Fast Pyrolysis in a Microfluidized Bed Reactor: Effect of Biomass Properties and Operating Conditions on Volatiles Composition as Analyzed by Online Single Photoionization Mass Spectrometry. *Energy Fuels* 2015, 29, 7364–7374.
- (23) Bobeldijk, M.; Van der Zande, W. J.; Kistemaker, P. G. Simple Models for the Calculation of Photoionization and Electron Impact Ionization Cross Sections of Polyatomic Molecules. *Chem. Phys.* 1994, 179, 125–130.
- (24) Zhou, Z.; Zhang, L.; Xie, M.; Wang, Z.; Chen, D.; Qi, F. Determination of Absolute Photoionization Cross-Sections of Alkanes and Cyclo-Alkanes. *Rapid Commun. Mass Spectrom.* 2010, 24, 1335–1342.
- (25) Yang, B.; Wang, J.; Cool, T. A.; Hansen, N.; Skeen S.; Osborn, D. L. Absolute photoionization cross-sections of some combustion intermediates. *Int. J. Mass Spectrom.* 2012, 309, 118–128.
- (26) Wang, J.; Yang, B.; Cool, T. A.; Hansen N.; Kasper T. Near-Threshold Absolute Photoionization Cross-Sections of Some Reaction Intermediates in Combustion. *Int. J. Mass Spectrom.* 2008, 269, 210–220.
- (27) Cool, T. A.; Nakajima, K.; Mostefaoui, T. A.; Qi, F.; Mclroy, A.; Westmoreland, P. R.; Law, M. E.; Poisson, L.; Peterka, D. S.; Ahmed, M. Selective Detection of Isomers with Photoionization Mass Spectrometry for Studies of Hydrocarbon Flame Chemistry. *J. Chem. Phys.* 2003, 119, 8356–8365.
- (28) Bahrini, C.; Herbinet, O.; Glaude, P.-A.; Schoemaeker, C.; Fittschen C.; Battin-Leclerc, F. Detection of Some Stable Species During the Oxidation of Methane by Coupling a Jet-Stirred Reactor (JSR) to cw-CRDS. *Chem. Phys. Lett.* 2012, 534, 1-7.
- (29) Rodriguez, A.; Frottier, O.; Herbinet, O.; Fournet, R.; Bounaceur, R.; Fittschen, C.; Battin-Leclerc, F. Experimental and Modeling Investigation of the Low-Temperature Oxidation of Dimethyl Ether. *J. Phys. Chem. A* 2015, 119, 7905–7923.
- (30) Morajkar, P. ; Schoemaeker, C.; Fittschen, C. Absolute Absorption Cross Sections for Two Selected Lines of Formaldehyde Around 6625 cm<sup>-1</sup>. *J. Mol. Spectrosc.* 2012, 281, 18–23.
- (31) Macko, P.; Romanini, D.; Mikhailenko, S. N.; Naumenko, O. V.; Kassi, S.; Jenouvrier, A.; Tyuterev, V. G.; Campargue, A. High sensitivity CW-Cavity Ring Down Spectroscopy of Water in the Region of the 1.5 μm Atmospheric Window. *J. Mol. Spectrosc.*, 2004, 227, 90–108.
- (32) Parker, A. E.; Jain, C.; Schoemaeker, C.; Szriftgiser, P.; Votava, O.; Fittschen, C. Simultaneous, Time-Resolved Measurements of OH and HO<sub>2</sub> Radicals by Coupling of High Repetition Rate LIF and cw-CRDS Techniques to a Laser Photolysis Reactor and Its Application to the Photolysis of H<sub>2</sub>O<sub>2</sub>. *Appl. Phys. B Lasers Opt.* 2011, 103, 725–733.
- (33) Wang, Z.; Zhao, L.; Wang, Y.; Bian, H.; Zhang, L.; Zhang, F.; Li, Y.; Sarathy, S. M.; Qi, F. Kinetics of Ethylcyclohexane Pyrolysis and Oxidation: An Experimental and Detailed Kinetic Modeling Study. *Combust. Flame* 2015, 162, 2873–2892.
- (34) Cooper, G.; Anderson, J. E.; Brion, C. E. Absolute Photoabsorption and Photoionization of Formaldehyde in the VUV and Soft X-Ray Regions (3–200 eV). *Chem. Phys.* 1996, 209, 61–77.

- (35) Montgomery, J. A., Jr; Frisch, M. J.; Ochterski, J. W.; Petersson, G. A. A Complete Basis Set Model Chemistry. VI. Use of Density Functional Geometries and Frequencies. *J. Chem. Phys.* 1999, 110, 2822-2827.
- (36) Frisch, M. J.; Trucks, G. W.; Schlegel, H. B.; Scuseria, G. E.; Robb, M. A.; Cheeseman, J. R.; Scalmani, G.; Barone, V.; Mennucci, B.; Petersson, G. A.; et al. Gaussian 09, Revision A.1; Gaussian, Inc.: Wallingford, CT, 2009. Gaussian 09; 2009.
- (37) El-Nahas, A. M.; Simmie, J. M.; Mangood, A. H.; Hirao, K.; Song, J.-W.; Watson, M. A.; Taketsugu, T.; Koga, N. Assessment of Hybrid, Meta-Hybrid-GGA, and Long-Range Corrected Density Functionals for the Estimation of Enthalpies of Formation, Barrier Heights, and Ionisation Potentials of Selected C1–C5 Oxygenates. *Molecular Physics* 2015, 113 (13–14), 1630–1635.
- (38) El-Nahas, A. M.; Mangood, A. H.; Takeuchi, H.; Taketsugu, T. Thermal Decomposition of 2-Butanol as a Potential Nonfossil Fuel: A Computational Study. *J. Phys. Chem. A* 2011, 115, 2837–2846.
- (39) Cuoci, A.; Frassoldati, A.; Faravelli, T.; Ranzi, E. OpenSMOKE++: An Object-Oriented Framework for the Numerical Modeling of Reactive Systems with Detailed Kinetic Mechanisms. *Comp. Phys. Com.* 2015, 192, 237–264.
- (40) Kee, R. J.; Ruplay, F. M.; Miller, J. A. Chemkin II. A Fortran Chemical Kinetics Package for the Analysis of a Gas-Phase Chemical Kinetics. Sandia Laboratories Report, S 89-8009B; Sandia National Laboratories: Albuquerque, NM, 1993.
- (41) Bugler, J.; Somers, K. P.; Silke, E. J.; Curran, H. J. Revisiting the Kinetics and Thermodynamics of the Low-Temperature Oxidation Pathways of Alkanes: A Case Study of the Three Pentane Isomers. *J. Phys. Chem. A* 2015, 119, 7510–7527.
- (42) Biet, J.; Hakka, M. H.; Warth, V.; Glaude, P.-A.; Battin-Leclerc, F. Experimental and Modeling Study of the Low-Temperature Oxidation of Large Alkanes. *Energy Fuels* 2008, 22, 2258–2269.
- (43) Baulch, D. L.; Cobos, C. J.; Cox, R. A.; Frank, P.; Hayman, G.; Just, Th.; Kerr, J. A.; Murrells, T.; Pilling, M. J.; Troe, J.; et al. Evaluated Kinetic Data for Combustion Modeling. Supplement I. *J. Phys. Chem. Ref. Data* 1994, 23, 847–848.
- (44) Zhou, C.-W.; Li, Y.; O'Connor, E.; Somers, K. P.; Thion, S.; Keese, C.; Mathieu, O.; Zhou, E.; Petersen, E. L.; DeVerter, T. A.; et al. A Comprehensive Experimental and Modeling Study of Isobutene Oxidation. *Combust. Flame* 2016, 167, 353–379.
- (45) Barbé, P.; Battin-Leclerc, F.; Côme, G. M. Experimental and Modelling Study of Methane and Ethane Oxidation Between 773 and 1573 K. *J. Chim. Phys.* 1995, 92, 1666–1692.
- (46) Goldsmith, C. F.; Klippenstein, S. J.; Green, W. H. Theoretical Rate Coefficients for Allyl + HO<sub>2</sub> and Allyloxy Decomposition. *Proc. Combust. Inst.* 2011, 33, 273–282.
- (47) Pelucchi, M.; Bissoli, M.; Cavallotti, C.; Cuoci, A.; Faravelli, T.; Frassoldati, A.; Ranzi, E.; Stagni, A. Improved Kinetic Model of the Low-Temperature Oxidation of n-Heptane. *Energy Fuels* 2014, 28, 7178–7193.